



VYSOKÉ UČENÍ TECHNICKÉ V BRNĚ

BRNO UNIVERSITY OF TECHNOLOGY

FAKULTA ELEKTROTECHNIKY A KOMUNIKAČNÍCH TECHNOLOGIÍ

FACULTY OF ELECTRICAL ENGINEERING AND COMMUNICATION

ÚSTAV RADIOELEKTRONIKY

DEPARTMENT OF RADIO ELECTRONICS

ENERGETICKÁ BILANCE UWC SPOJE

ENERGY BALANCE OF THE UWC LINK

DIPLOMOVÁ PRÁCE

MASTER'S THESIS

AUTOR PRÁCE

AUTHOR

Bc. Jan Bartoň

VEDOUcí PRÁCE

SUPERVISOR

doc. Ing. Lucie Hudcová, Ph.D.

BRNO 2024



Diplomová práce

magisterský navazující studijní program **Elektronika a komunikační technologie**

Ústav radioelektroniky

Student: Bc. Jan Bartoň

ID: 221048

Ročník: 2

Akademický rok: 2023/24

NÁZEV TÉMATU:

Energetická bilance UWC spoje

POKYNY PRO VYPRACOVÁNÍ:

MP(K)C-M2E: Seznamte se s optickými bezkabelovými spoji provozovanými pod vodní hladinou (Underwater Communications UWC). Popište vlastnosti vodního přenosového prostředí pro optickou oblast spektra. Definujte útlumové charakteristiky vodního prostředí, stanovte míru vlivu šumů pro UWC a zaměřte se na popis turbulentního proudění, které způsobuje vodní turbulenci. Stanovte charakter interakce mezi optickým svazkem a vodním přenosovým prostředím. Navrhněte postup a následně program pro určení míry vlivu vodní turbulence na optický svazek. Do programu implementujte modul pro výpočet útlumu optického signálu vodním prostředím. MP(K)C-MSE: Vytvořte komplexní program pro výpočet energetické bilance podvodního zdroje. Program bude umožňovat definici zdroje a detektoru záření. Pro vstupní data pro výpočty využijte dostupné globální datasey. V kalkulaci zohledněte i šum pozadí.

DOPORUČENÁ LITERATURA:

- [1] H. Kaushal and G. Kaddoum, "Underwater Optical Wireless Communication," in IEEE Access, vol. 4, pp. 1518-1547, 2016, doi: 10.1109/ACCESS.2016.2552538.
- [2] G. Song and J. Xu, "Review on Long-distance Underwater Wireless Optical Communication," 2021 19th International Conference on Optical Communications and Networks (ICOON), Qufu, China, 2021, pp. 1-4, doi: 10.1109/ICOON53177.2021.9563681.

Termín zadání: 16.2.2024

Termín odevzdání: 20.5.2024

Vedoucí práce: doc. Ing. Lucie Hudcová, Ph.D.

doc. Ing. Lucie Hudcová, Ph.D.

předseda rady studijního programu

UPOZORNĚNÍ:

Autor diplomové práce nesmí při vytváření diplomové práce porušit autorská práva třetích osob, zejména nesmí zasahovat nedovoleným způsobem do cizích autorských práv osobnostních a musí si být plně vědom následků porušení ustanovení § 11 a následujících autorského zákona č. 121/2000 Sb., včetně možných trestněprávních důsledků vyplývajících z ustanovení části druhé, hlavy VI. díl 4 Trestního zákoníku č. 40/2009 Sb.

Abstrakt

Tato diplomová práce je zaměřená na popis šíření optického svazku podvodním prostředím se zaměřením na vliv turbulentního proudění na odsměrování svazku. V první části práce je poskytnut popis vlastností podvodního prostředí a jejich vliv na optický svazek. V druhé části jsou prezentovány metody použitelné pro výpočet útlumu podvodního prostředí, zaměřující se na popis turbulentního prostředí. Ve třetí části je představena softwarová implementace algoritmu popsaného ve druhé části. Výsledkem práce je postup výpočtu šíření optického svazku podvodním prostředím a jeho softwarová implementace.

Klíčová slova

Turbulence, podvodní prostředí, optický svazek, útlum, odsměrování, šum, chlorofyl, absorpce, rozptyl, ABCD matice, koeficient extinkce.

Abstract

This master's thesis is aimed at the description of the optical ray propagation through underwater environment, focusing mainly on the optical beam's deflection by a turbulent space. In the first part of the thesis, the description of the properties of underwater environment and their impact on the optical beam is presented. In the second part, methods usable for the calculation of attenuation of an underwater environment are presented, focusing on the turbulent environment. In the third part, the software implementation of the algorithm presented in the second part is presented. The outcome of this thesis is a procedure for calculating the propagation of the optical beam through an underwater environment and its software implementation.

Keywords

Turbulence, underwater environment, optical beam, attenuation, deflection, noise, chlorophyll, absorption, scattering, ABCD matrices, extinction coefficient.

Bibliografická citace

BARTOŇ, Jan. *Energetická bilance UWC spoje*. Brno, 2024. Dostupné také z: <https://www.vut.cz/studenti/zav-prace/detail/153505>. Diplomová práce. Vysoké učení technické v Brně, Fakulta elektrotechniky a komunikačních technologií, Ústav radioelektroniky. Vedoucí práce Lucie Hudcová.

Prohlášení autora o původnosti díla

Jméno a příjmení studenta: *Jan Bartoň*

VUT ID studenta: *221048*

Typ práce: *Diplomová práce*

Akademický rok: *2023/24*

Téma závěrečné práce: *Energetická bilance UWC spoje*

Prohlašuji, že svou závěrečnou práci jsem vypracoval samostatně pod vedením vedoucí/ho závěrečné práce a s použitím odborné literatury a dalších informačních zdrojů, které jsou všechny citovány v práci a uvedeny v seznamu literatury na konci práce.

Jako autor uvedené závěrečné práce dále prohlašuji, že v souvislosti s vytvořením této závěrečné práce jsem neporušil autorská práva třetích osob, zejména jsem nezasáhl nedovoleným způsobem do cizích autorských práv osobnostních a jsem si plně vědom následků porušení ustanovení § 11 a následujících autorského zákona č. 121/2000 Sb., včetně možných trestněprávních důsledků vyplývajících z ustanovení části druhé, hlavy VI. díl 4 Trestního zákoníku č. 40/2009 Sb.

V Brně dne: 19. května 2024

podpis autora

Poděkování

Děkuji vedoucí diplomové práce doc. Ing. Lucii Hudcové, PhD. za účinnou metodickou, pedagogickou, morální a odbornou pomoc a další cenné rady při zpracování mé diplomové práce.

V Brně dne: 19. května 2024

podpis autora

Content

1. CHARACTERISTICS OF AN UNDERWATER ENVIRONMENT	12
1.1 ATTENUATION.....	12
1.2 SCATTERING AND ABSORPTION	12
1.3 TURBULENCE	14
1.4 BACKGROUND NOISE.....	15
1.4.1 Shot noise.....	15
1.4.2 Thermal noise.....	15
1.4.3 Fading.....	15
1.4.4 Multipath interference.....	16
1.4.5 Solar noise	16
1.4.6 Chlorophyll concentration.....	16
2. COMPUTATION OF THE SIGNAL ATTENUATION UNDER WATER	18
2.1 ATTENUATION BY ABSORPTION AND SCATTERING.....	18
2.1.1 Total absorption coefficient	18
2.1.2 Total scattering coefficient.....	20
2.1.3 Power received by the receiver.....	21
2.2 TURBULENCE	22
2.2.1 Snell's law	22
2.2.2 ABCD matrices	23
2.2.3 Received power calculation	26
2.3 SOLAR RADIATION.....	30
2.4 OPTICAL LINK BUDGET.....	30
2.5 MODULATION SCHEME.....	31
2.5.1 On-off keying (OOK).....	31
2.5.2 Pulse amplitude modulation (PAM).....	31
2.5.3 Pulse position modulation (PPM).....	32
3. SOFTWARE IMPLEMENTATION.....	33
3.1 PROGRAM DESCRIPTION	33
3.1.1 Database	34
3.1.1.1 Lenses	34
3.1.1.2 Cover windows.....	35
3.1.1.3 Transmitters	35
3.1.1.4 Filters	36
3.1.1.5 Receivers.....	36
3.1.2 Definition of environment	37
3.1.2.1 Transfer chain definition	37
3.1.2.2 Transmission medium definition.....	38
3.1.2.3 Wavelength tool	40
3.1.2.4 Modulation scheme selection	41
3.1.3 Results.....	42
3.1.4 Information about the program.....	44
3.1.5 Suggested procedure for link design	45
3.2 MODEL SITUATIONS	46
3.2.1 Example situation 1.....	46
3.2.2 Example situation 2.....	49
3.2.3 Example situation 3.....	51

4. CONCLUSION..... 53

LIST OF IMAGES

Figure 1: Depth dependent concentration of chlorophyll C_c , for water type 5 (left side) and depth and water type dependent concentration of chlorophyll C_c (right side).....	17
Figure 2: Wavelength dependency of clear water absorption coefficient, adapted from [23].	19
Figure 3: Wavelength λ and chlorophyll concentration C_c dependent chlorophyll attenuation coefficient a_c	20
Figure 4: Calculation of the turbulent beam deflection using Snell's law.	23
Figure 5: Calculation of the turbulent beam deflection using Ray tracing matrices.	24
Figure 6: Illustrative model of N turbulent cells chained together representing a turbulent space.	25
Figure 7: Visualization of the beam deflection while propagating through a 3D turbulent space.	26
Figure 8: Visualization of the incidence angle ψ calculation from calculated deflection vectors in x and y axes, z is the optical axis of the system.	29
Figure 9: 3D representation of the beam deflection, red circle is the receiving lens, black line is the optical axis and the contour is the gaussian beam profile (left side), XY cut in height $z = 0,5$ of the graph on the left side, showing beam's deflection vector \mathbf{v} (red) and the gaussian beam deflection (blue circle), the optical axis points outwards from point $[0, 0]$ (right side).	29
Figure 10: Visualization of optical link budget calculation, z is the distance from the transmitter.	31
Figure 11: Achievable BER for attained SNR	32
Figure 12: Title page of the program.	33
Figure 13: Detail of the overhead menu.....	33
Figure 14: Menu item "database".	34
Figure 15: Database of lenses window.	34
Figure 16: Database of cover windows window.	35
Figure 17: Database of transmitters window.	35
Figure 18: Database of filters window.	36
Figure 19: Database of receivers window.....	36
Figure 20: Menu item "Definition".....	37
Figure 21: Transfer chain definition window.	37
Figure 22: Transmission medium definition window.	38
Figure 23: Choice of a geographical location window.	39
Figure 24: Date and time selection window.....	39
Figure 25: Turbulence strength settings window.	40
Figure 26: Description of turbulent parameters window.	40
Figure 27: Wavelength tool window showing 2D graphs.....	41
Figure 28: Wavelength tool window showing 3D graphs.....	41
Figure 29: Modulation scheme selection window.	42
Figure 30: Menu item "Results".	42
Figure 31: Results of the calculations window.	43
Figure 32: Menu item "Help".	44
Figure 33: Window with information about the program.	44
Figure 34: Calculated link budget after the first iteration (left side), calculated histogram for turbulent attenuations (right side).	46
Figure 35: Calculated beam wandering after the first iteration (top side), calculated parameters of the link (bottom side).	47
Figure 36: Calculated link budget after the second iteration (left side), calculated histogram for turbulent attenuations (right side).	47

Figure 37: Calculated beam wandering after the second iteration (top side), calculated parameters of the link (bottom side).	48
Figure 38: Calculated link budget after the first iteration (left side), calculated histogram for turbulent attenuations (right side).	49
Figure 39: Calculated beam wandering after the first iteration	49
Figure 40: Calculated link budget after the second iteration (left side), calculated histogram for turbulent attenuations (right side).	50
Figure 41: Calculated parameters of the link.	50
Figure 42: Calculated link budget after the first iteration (left side), calculated histogram for turbulent attenuations (right side).	51
Figure 43: Calculated beam wandering after the first iteration.	51
Figure 44: Calculated link budget after the second iteration (left side), calculated histogram for turbulent attenuations (right side).	52
Figure 45: Calculated parameters of the link.	52
Figure 46: Flowchart of the algorithm for calculating turbulent optical ray attenuation.	60

INTRODUCTION

The vast majority of communication taking place on Earth is nowadays realised via wireless links through the Earth's atmosphere. As the atmosphere consists of air, whose properties are similar to that of vacuum, it doesn't impose as big of a challenge to design a wireless link as it does in an underwater environment.

With the technological advancement of humankind, it is now possible to venture even into the most hostile of territories among which the underwater environment can be included. To communicate in such an environment, it would be impractical to use wired links, as it would need to follow the oceans bed and the links would be extremely long and costly. It would also be challenging to communicate with ships or other objects floating on the ocean's surface or to establish communication between for example two moving submarines or to communicate with aircraft. That's one of the reasons why underwater wireless links are getting more attention nowadays. The concept of wireless underwater communication is not new, experiments with wireless underwater links using radiofrequency or acoustic waves have been conducted since the second world war. With the recent technological advancements though, it has become possible to realise the communication with the help of optical waves. One of its greatest advantages over other wireless technology is its wide bandwidth and thus its potential to send information at high speeds. A lot of researchers now focus their attention at this topic to make it possible for the communication to be feasible at longer distances than today.

This thesis is aimed at the task of describing the attenuation characteristics of an underwater environment and at the process of designing an optical underwater wireless link and calculating its budget and is divided into four chapters.

In the first chapter the aspects of underwater communication are investigated, a brief description on how the propagating optical beam is influenced by turbulence and attenuation is provided and the kinds of background noises present in the communication channel are presented along with the description of chlorophyll concentration profile.

In the second chapter detailed procedure on how to include the aspects mentioned in the first chapter into the calculations of optical ray propagation is provided. Two possible methods that can be used to calculate the optical ray propagation through turbulence are described. The problematics of an optical link budget is mentioned. At the end of this chapter a brief summary of the most often used digital modulations in optical communications is provided.

In the third chapter, the software implementation of the procedures presented in the previous chapter is described along with the user interface description. Three model situations are shown and with the help of the program, parameters of the link of desired parameters are evaluated.

In the conclusion, the results of this thesis are discussed.

1. CHARACTERISTICS OF AN UNDERWATER ENVIRONMENT

The propagation of an optical beam through the underwater environment is much more influenced by its surroundings, than it would be in case of an atmospheric link. This is caused by various physical processes happening under water which are going to be described in this chapter.

1.1 Attenuation

When an optical ray does not propagate through free space, the ray gets attenuated the more the further it travels. The attenuation L [dB/km] (or [dB/m] in case of media with stronger signal attenuation, which is the case of water) is dependent on various properties of the propagating medium. Accurately calculating the attenuation in an underwater environment is no easy task, as the conditions under water are very dynamic and fluctuate frequently. It is not possible with current computational power to precisely calculate the attenuation dynamically, so instead a statistical approach is used, which estimates the values based on their probabilities.

The attenuation depends on the concentration of substances dissolved in the water, geographical position, temperature and the depth of the water, wavelength of the optical carrier, concentration of water organisms and the turbidity.

1.2 Scattering and absorption

Scattering and absorption are the two physical processes, responsible for the attenuation and deflection of an electromagnetic wave propagating through a material medium. Absorption is the process in which a photon is absorbed by a molecule, out of which the medium consists, and its energy is then transformed into thermal energy, which heats the medium up. The molecular absorption can be described by a variation of the dielectric constant, which depends on the photon's frequency. At lower frequencies, the absorption coefficient is proportional to $\sqrt{\omega}$, as water behaves like a conductor. At higher frequencies, the attenuation coefficient is given by

$$\chi_a(\omega) \cong \frac{\Im(\epsilon(\omega))}{\sqrt{\Re(\epsilon(\omega))}} \cdot \frac{\omega}{c}, \quad (1.1)$$

where $c = 3 \cdot 10^8 \text{ m} \cdot \text{s}^{-1}$ and $\epsilon(\omega)$ is the frequency dependent permittivity and can be estimated using experimental data or using a proper quantum-mechanical model of the medium, see [5].

The frequency at which water stops behaving like a conductor and starts to behave like a dielectric instead is called the plasma frequency and can be found using the following formula [5]

$$\omega_p^2 = \frac{4\pi NZe^2}{m}, \quad (1.2)$$

where Z [-] is the number of atoms, m is the mass of electron and e is its charge. For seawater, the plasma frequency is about 250 GHz.

Scattering, on the other hand causes the absorbed photon to be re-emitted either elastically, with the same energy and so with the same wavelength but under a different angle (Rayleigh's scattering), or with lower energy and under a different angle (Raman's scattering), which also causes a change in the photon's wavelength. If we also consider some larger objects, where the wavelength of the photon is comparable to the size of the obstacle, Mie's scattering should be taken into account as well.

The scattering coefficient, if the variations in temperature are neglected, is given by formula for Rayleigh's scattering [5]

$$\chi_s \cong \frac{k^4}{6\pi \cdot N} |\epsilon - 1|^2, \quad (1.3)$$

where k [$\text{rad} \cdot \text{m}^{-1}$] is the wavenumber, ϵ [$\text{F} \cdot \text{m}^{-1}$] is the permittivity and N [-] is the number of molecules.

The scattering coefficient is also affected by various particles, water organisms and gelbstoffe¹. If we want to account for influence of said factors, the most accurate way would be to approximate them by spheres of corresponding radiuses and calculate the scattering coefficient using Mie's theorem, which is quite complicated and can be found in [5].

In practical situations, earlier mentioned theorems are usually not used for optical ray attenuation's calculation, because the amount and distribution of obstacles the optical beam interacts with is not known. Rather a simplified approach is used, where the attenuation is calculated from [5]

$$c(\lambda) = a(\lambda) + b(\lambda), \quad (1.4)$$

where c is the beam extinction coefficient, is frequency dependent and consists of coefficients $a(\lambda)$ and $b(\lambda)$ that represent the overall absorption and scattering, respectively. The propagation loss is then also dependent on the wavelength and distance z and is given as [5]

$$L_p(\lambda, z) = e^{-c(\lambda)z}. \quad (1.5)$$

¹ German word, describing organic matter that causes a yellowing tint of the water [4]

where $c(\lambda)$ is the beam extinction coefficient and z is the distance from the source to the receiver.

1.3 Turbulence

Another crucial factor that needs to be considered when designing an underwater optical link is turbulence. It can be described as a fluctuation of refraction index caused by variations in temperature, salinity and pressure along the propagation path which causes the optical ray to be deflected due to refraction and at the receiver only a fraction of the optical intensity is received by the receiving lens causing the received power to fluctuate. This phenomenon is called scintillation and degrades the system's performance [5].

Mathematically, turbulence is described by Navier Stoke's differential equations, whose exact solution is yet to be found and so they either need to be solved numerically or another approach needs to be taken when calculating it's influence on the propagation of the optical beam.

The turbid area can be divided into cells, that are considered to have a constant refractive index. Because the turbulence is by no means a stationary phenomenon, the refractive index of each cell varies with time and so do the values of respective refractive indexes. Statistical approach is once more utilised, where the value of a particular refractive index at a given time is estimated from its distribution function obtained from measurements. Depending on the dimensions of each cell, they can be approximated either as a volume with constant refractive index or as two lenses separated once again with a volume of constant refractive index. The refractive index of water can be approximated according to an empirically derived formula as in Eq. (1.6) or Eq. (1.7), depending on if the influence of temperature is to be included into calculations

$$n(\lambda) \cong 1,31848 + \frac{6,662}{\lambda[\text{nm}] - 129,2}, \quad (1.6)$$

$$n(\lambda, t) \cong A(t) + \frac{B(t)}{\lambda^2} + \frac{C(t)}{\lambda^4} + \frac{D(t)}{\lambda^6}, \quad (1.7)$$

where λ [m] is the wavelength of the light and $A(t), B(t), C(t), D(t)$ are Cauchy coefficients [24], [25]. As can be seen from Fig. 2 and 3, the used wavelength for underwater communication will be chosen as such as for the optical beam to be the least attenuated. The smallest attenuation of clear water is around 400 to 500 nm, whereas waters with the presence of chlorophyll has the smallest attenuation at around 500 to 600 nm, which means, that if the communication is to take places in clear water, wavelength from the blue spectral region will be selected, if chlorophyll presence is expected, the wavelength will move towards the green area of the optical spectrum.

An alternative, purely statistical approach can be utilised, when calculating the turbulent attenuation under water. In free space optics, turbulent attenuation can be easily calculated using Kolmogorov spectrum model. As the mechanics of underwater

turbulence is quite similar to the atmospheric turbulence, the same model can be used under water as well. The downside of this method is, that it does not take into consideration the size of the receiving optics, whereas another method, similar to Kolmogorov spectrum model, Andrew's model, employs the size of the receiving optics into the calculations. Both of those methods rely on structural refractive index parameter C_n^2 , representing the volume of turbulence. More information on this topic can be found in [3], [15].

1.4 Background noise

In a perfect world, where a completely dark optical channel containing no external photons exists and hence no sources of noise are present, it would be possible to communicate at almost infinite distances because there would be no limit for power needed to be present at the detector for the transmitted signal to be successfully decodable. In real-world applications though, every photodetector has a power threshold below which the optical signal cannot be received as it gets lost in noise. This threshold depends on the type of photodetector used. There are multiple sources of noise that can be present in the optical communication channel, listed below.

1.4.1 Shot noise

Shot noise is caused by the fact that electric current is conveyed by electrons that are generated at random times. It is a stationary random process with Poisson statistics which generates additive current in response to electric current flowing through a semiconductor. *Dark current*, which is the amount of electric current flowing through a photodetector when no illumination is present, also contributes to shot noise and needs to be included into the noise threshold calculations. More on this topic can be found in [17].

1.4.2 Thermal noise

In a conductor whose temperature is greater than 0 K, electrons move randomly causing the current flowing through the conductor to fluctuate. The fluctuations of the current are modelled by an additive current called *thermal current*, which can be mathematically described as a stationary Gaussian random process, with almost constant spectral density, approximately up to frequency $f = 1$ GHz, which makes it behave almost as white noise. More on this topic can be found in [17].

1.4.3 Fading

Fading is a process, in which the amount of power received by the receiver varies with time due to variations in the communication channel. In case of underwater optical communications, fading mostly happens due to changes in refractive index (turbulence) or reflections from surfaces, for example ocean bed, from the surface of the ocean or from foreign objects under water. If a direct line of sight path exists between the transmitter and the receiver, such channel is called Rayleigh channel, whereas a channel with no direct line of sight path is called Rician channel. More can be found in [18], [19].

1.4.4 Multipath interference

When the optical ray propagates from the transmitter towards the receiver along multiple paths with various lengths, the time at which the optical ray arrives to the receiver after individual paths is not the same, which causes the individual received components to interfere with each other and the carried information can be lost. This phenomenon can be suppressed by using an adequate modulation scheme or by placing the communication channel far enough from reflective surfaces. More on this topic can be found in [20].

1.4.5 Solar noise

Solar noise is caused by the sun shining on the surface of the ocean or another body of water. While some of the light is reflected away from the surface of the body of water, most of it continues to propagate inside. The solar power is quickly attenuated under water and the attenuation is proportional to the concentration of chlorophyll. If the receiver is oriented towards the surface of the body of water and is not far enough from the surface, it can get saturated merely by the solar noise and no information can be transferred via the communication channel. Solar noise can be suppressed using a band-pass filter before the receiver of bandwidth $\Delta\lambda$ to let only the desired wavelength pass.

1.4.6 Chlorophyll concentration

The concentration of chlorophyll is dependent on the depth under water. It starts to increase going deeper from the surface of the body of water until it reaches a maximum called *deep chlorophyll maximum* (DCM) [12], below which the concentration starts to decrease again. The reason for this distribution profile is biological, as just below the surface are not enough nutrients for the organisms to survive and deeper in the water are no light sources, except for bioluminescence, which is needed by the phytoplankton to perform photosynthesis. [12]

The depth dependency of chlorophyll concentration can be approximated by an empirically derived formula [12], as in Eq. (1.8)

$$C_c(z) = B_0 + S \cdot z + \frac{h}{\sigma\sqrt{2\pi}} e^{-\frac{(z-z_{max})^2}{2\sigma^2}}, \quad (1.8)$$

where the B_0 is the background chlorophyll concentration on the surface, S is the vertical gradient, which is always negative, as the chlorophyll concentration decreases with increasing depth, h is the total chlorophyll concentration, z_{max} is the depth at which the DCM is located and σ is the standard deviation of chlorophyll concentration defined as in Eq. (1.9) [12]

$$\sigma = \frac{h}{\sqrt{2\pi(C_{c,z_{max}} - B_0 - S \cdot z_{max})}}, \quad (1.9)$$

where $C_{c_{z_{max}}}$ [$\text{mg} \cdot \text{m}^{-3}$] is the maximal chlorophyll concentration at the DCM point. The calculated depth dependent profiles by the software implementation are depicted in Fig. 1.

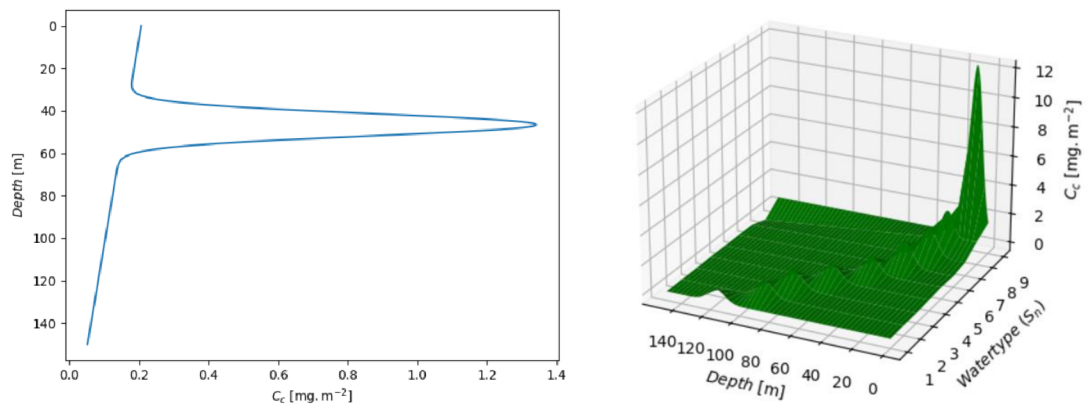


Figure 1: Depth dependent concentration of chlorophyll C_c , for water type 5 (left side) and depth and water type dependent concentration of chlorophyll C_c (right side).

2. COMPUTATION OF THE SIGNAL ATTENUATION UNDER WATER

2.1 Attenuation by absorption and scattering

The overall attenuation will be calculated using the above-mentioned equations (1.4) and (1.5). Depending on the type of water being considered, the appropriate relation will be considered to determine the scattering coefficient $b(\lambda)$. To calculate the absorption coefficient $a(\lambda)$ and the subsequent scattering coefficients, it is first necessary to evaluate the concentrations of particles responsible for the absorption and scattering of the optical power. Those values can be found from measurements.

2.1.1 Total absorption coefficient

The overall absorption in sea water is caused by various factors and so all of them need to be included into the calculation

$$a(\lambda) = a_w(\lambda) + a_{phy}(\lambda) + a_g(\lambda) + a_n(\lambda), \quad (2.1)$$

where the overall absorption coefficient $a(\lambda)$ [m^{-1}] consists of absorption by clear water $a_w(\lambda)$, absorption by phytoplankton $a_{phy}(\lambda)$, absorption by gelbstoffe $a_g(\lambda)$ and of absorption by non-algae materials $a_n(\lambda)$. [5], [6].

The absorption by other non-algal materials $a_n(\lambda)$ will be neglected in future computations because it is dependent on the geographical position which will not be taken into account.

The absorption by gelbstoffe and by phytoplankton can be calculated using simplified approach called One-parameter attenuation model [11], which relates the absorption by gelbstoffe and phytoplankton to the chlorophyll concentration. The absorption by gelbstoffe $a_g(\lambda)$ is caused by humic and fulvic acids produced by decaying organic matter and can be calculated as in Eq. (2.2)

$$a_g(\lambda) = a_f^0 C_f e^{-k_f \lambda} + a_h^0 C_h e^{-k_h \lambda}, \quad (2.2)$$

where $a_f^0 = 35,959 \text{ m}^2 \cdot \text{mg}^{-1}$ is a specific absorption coefficient of fulvic acid, $a_h^0 = 18,828 \text{ m}^2 \cdot \text{mg}^{-1}$ is a specific absorption coefficient of humic acid, C_f [$\text{mg} \cdot \text{m}^{-3}$], is the concentration of fulvic acid and C_h [$\text{mg} \cdot \text{m}^{-3}$], is the concentration of humic acid, $k_f = 0,0189 \text{ nm}^{-1}$ and $k_h = 0,01105 \text{ nm}^{-1}$ are the exponential coefficients of the respective acids [12]. Concentrations of acids can be calculated from chlorophyll concentration, as in Eq. (2.3) and (2.4)

$$C_f = 1,74098 \cdot C_c \cdot e^{0,12327 \cdot C_c}, \quad (2.3)$$

$$C_h = 0,19334 \cdot C_c \cdot e^{0,12343 \cdot C_c}, \quad (2.4)$$

where C_c [$\text{mg} \cdot \text{m}^{-3}$] is the chlorophyll concentration. The absorption by phytoplankton $a_{phy}(\lambda)$ can be calculated as in Eq. (2.5)

$$a_{phy}(\lambda) = a_c^0(\lambda) \left(\frac{C_c}{C_0} \right)^{0,602}, \quad (2.5)$$

where $a_c^0(\lambda)$ is a specific absorption coefficient of chlorophyll, C_c is the chlorophyll concentration and $C_0 = 1 \text{ mg} \cdot \text{m}^{-3}$ is a reference value. The specific absorption coefficient of chlorophyll can be calculated as in Eq. (2.6)

$$a_c^0(\lambda) = A(\lambda) \cdot C_c^{-B(\lambda)}, \quad (2.6)$$

where $A(\lambda)$ and $B(\lambda)$ are wavelength-dependent empirical coefficients obtained from measurements and can be found in [13]. And C_c is the concentration of chlorophyll.

The absorption coefficient of clear water $a_{cw}(\lambda)$ can be found from measurements, as in Fig. 2.

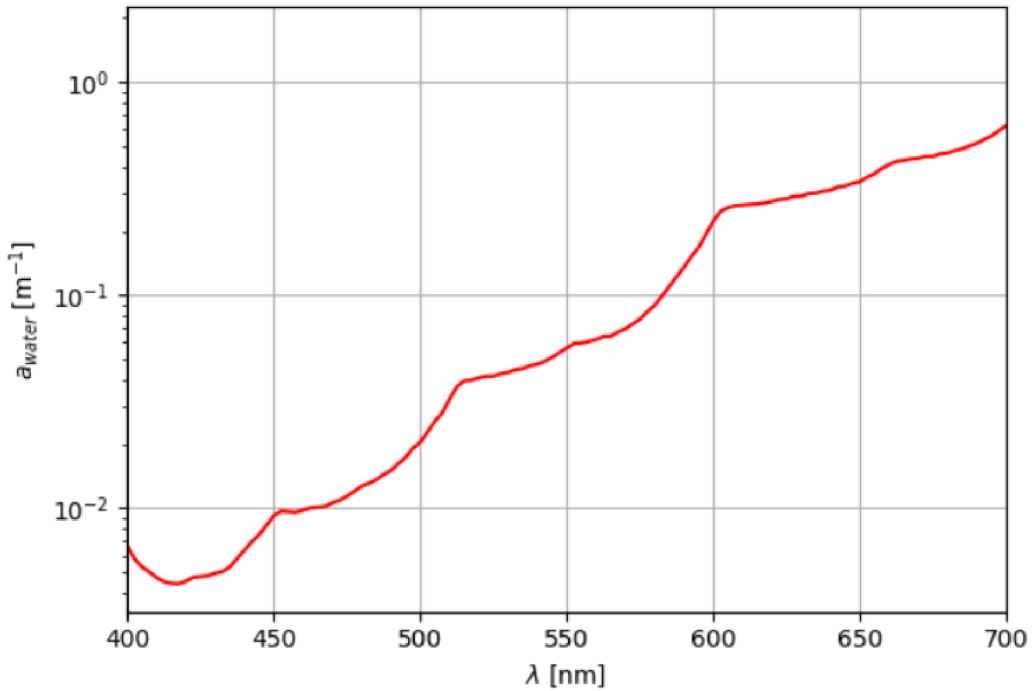


Figure 2: Wavelength dependency of clear water absorption coefficient, adapted from [23].

The absorption coefficient of chlorophyll $a_c^0(\lambda)$, calculated according to Eq. (2.6) and measured wavelength dependent coefficients from [13], can be seen in Fig. 3.

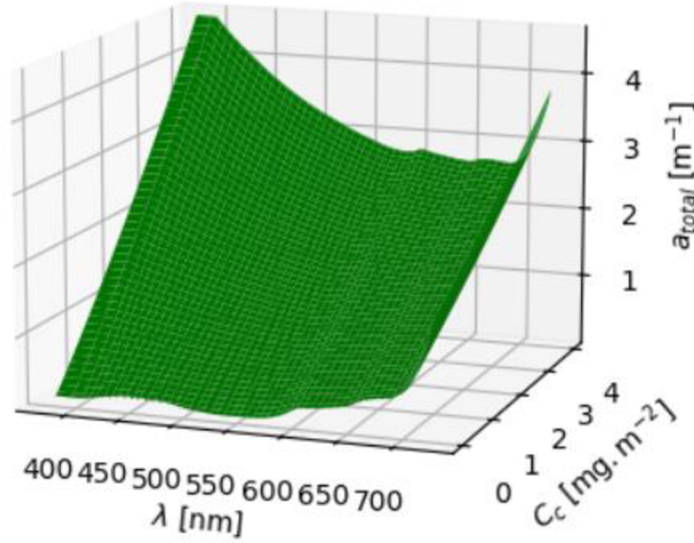


Figure 3: Wavelength λ and chlorophyll concentration C_c dependent chlorophyll attenuation coefficient a_c .

2.1.2 Total scattering coefficient

To calculate the coefficient $b(\lambda)$ [m^{-1}], representing the overall scattering properties of the water, it is first necessary to determine what kind of water the communication takes place in. If it is a region with pure sea water, the overall attenuation is dominated by absorption, as almost no particles are present, only particles smaller than the used wavelength, whose scattering properties are described by Rayleigh's scattering coefficient $b_{cw}(\lambda)$ given as

$$b_{cw}(\lambda) = 0,005826 \left(\frac{400}{\lambda} \right)^{4,322}, \quad (2.7)$$

where λ is the used wavelength of the light. If it is a region near land however, scattering starts to play a significant role, as larger particles are present there as well as the smaller particles. In this case the scattering properties of such waters are described by Mie's scattering, whose coefficient $b_l(\lambda)$ and $b_s(\lambda)$ for larger and smaller particles are given as in Eq. (2.8) and (2.9)

$$b_l(\lambda) = 1,151302 \left(\frac{400}{\lambda} \right)^{1,17}, \quad (2.8)$$

$$b_s(\lambda) = 0,341074 \left(\frac{400}{\lambda} \right)^{0,3}, \quad (2.9)$$

where λ is the wavelength.

Afterwards all of those subsequent scattering coefficients can be combined together to determine the total scattering coefficient $b(\lambda)$, as in Eq. (2.10)

$$b(\lambda) = b_{cW}(\lambda) + b_l(\lambda) \cdot C_L + b_s(\lambda) \cdot C_S, \quad (2.10)$$

where $b_{cW}(\lambda)$, $b_l(\lambda)$ and $b_s(\lambda)$ are the subsequent scattering coefficients and C_S and C_L are the respective concentrations of particles, that can be determined from the chlorophyll concentration C_C , as in Eq. (2.11) and (2.12)

$$C_S = 0,01739 \cdot C_C \cdot e^{0,11631 \cdot C_C}, \quad (2.11)$$

$$C_L = 0,76284 \cdot C_C \cdot e^{0,03092 \cdot C_C}, \quad (2.12)$$

where C_C is the concentration of chlorophyll.

2.1.3 Power received by the receiver

The power received by the receiver, after the optical beam has been subjected to turbulent deflection, absorption and scattering, can be expressed as

$$P_{RX}(\lambda, z) = H_0 \cdot P_0 \cdot e^{-c(\lambda)z}, \quad (2.13)$$

where z is the distance from the transmitter to the receiver, $c(\lambda)$ is the extinction coefficient calculated as in Eq. (1.4), P_0 is the power integrated by the receiving lens, calculated according to Eq. (2.28) and H_0 is the DC gain of the communication channel, that is defined as in Eq. (2.14) [22]

$$H_0 = \begin{cases} \frac{m+1}{2\pi} \cos^m(\phi) \frac{A_{PD}}{z} T_s(\psi) g(\psi) \cos(\psi), & \text{if } 0 \leq \psi \leq \psi_c, \\ 0, & \text{if } \psi > \psi_c \end{cases}, \quad (2.14)$$

where A_{PD} is the area of the photodetector, z is the distance from the transmitter to the receiver, $T_s(\psi)$ is the average filter transmission over the filter wavelength range $\Delta\lambda$ for a given incidence angle ψ , $g(\psi)$ is the gain of the receiver, for a given incidence angle ψ , defined as in Eq. (2.15) power, n is the internal refractive index and m is the *Lambertian order* defined as in Eq. (2.16) [22]

$$g(\psi) = \begin{cases} \frac{n^2}{\sin^2(\psi)}, & \text{if } 0 \leq \psi \leq \psi_c, \\ 0, & \text{if } \psi > \psi_c \end{cases}, \quad (2.15)$$

$$m = -\frac{\ln(2)}{\ln(\cos(\phi_{1/2}))}, \quad (2.16)$$

where $\phi_{1/2}$ is the semi-angle of the transmitter at half-power. The incident angle ψ must be greater than zero and lower than ψ_c which is the critical angle, above which the optical

ray is completely reflected from the surface² and no power is received [22]. The incident angle can be calculated from the angles at which the optical ray leaves the turbulence in x and y axis, as in Eq. (2.38).

2.2 Turbulence

To calculate the power received by the receiving lens at the receiver it is necessary to first determine the distance by which the beam is deflected from the optical axis of the system, after propagating through the system of turbulent cells. For this task, following methods can be used.

2.2.1 Snell's law

The simplest way to describe the turbulent area, is to consider it a homogenous area with a constant refractive index n_2 . In this case, beam deflection due to propagation through turbulence can be easily calculated using Snell's law (2.17).

$$n_1 \cdot \sin \alpha = n_2 \cdot \sin \beta, \quad (2.17)$$

where n_1 is the refractive index of the environment before the turbulent cell and n_2 is the refractive index of the turbulent cell itself.

Optical ray propagating from the environment with refractive index n_1 into the turbulent cell at an angle α is refracted at the interface of the cell to a lesser or a greater angle β with respect to the primary optical axis. Whether the angle β is greater or lesser than α depends on the ratio of refractive indexes $\frac{n_1}{n_2}$ (2.18). At the end of the turbulent cell, the optical ray is refracted once again at the second interface with respect to the secondary optical axis. If the two environments before and after the turbulent cell have the same refractive index, the angle at which the optical ray enters the turbulence is the same as the angle at which the optical ray leaves the turbulence. This principle can be seen in Fig. 4.

$$\beta \dots \begin{cases} \beta > \alpha, \text{ for } \frac{n_1}{n_2} > 1 \\ \beta = \alpha, \text{ for } n_1 = n_2 \\ \beta < \alpha, \text{ for } 0 < \frac{n_1}{n_2} < 1 \end{cases} . \quad (2.18)$$

Using Snell's law and trigonometric functions, formula for the deflection distance y_a can be derived

$$y_a = L \cdot tg \left(\arcsin \left(\frac{n_1}{n_2} \sin(\alpha) \right) \right). \quad (2.19)$$

² Also called *Total Internal Reflection* (TIR)

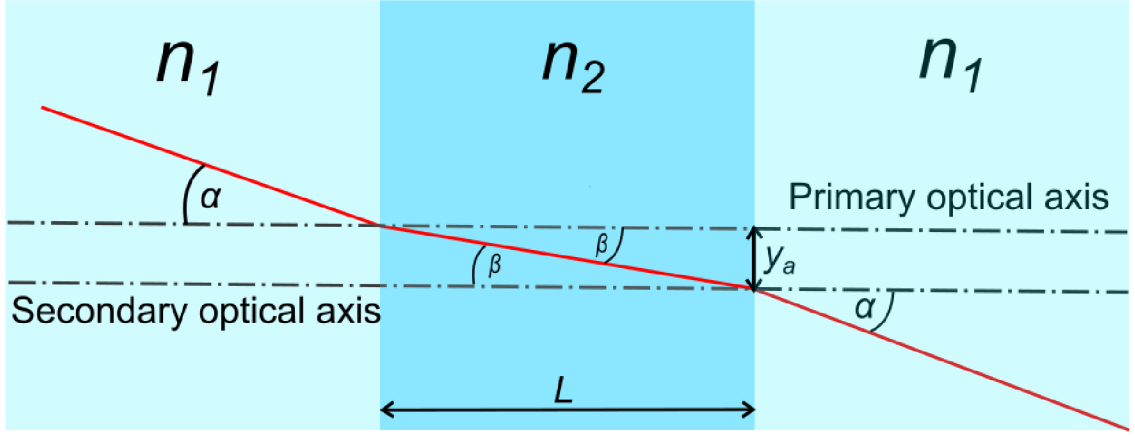


Figure 4: Calculation of the turbulent beam deflection using Snell's law.

In most practical situations, this approach cannot be used, as the turbulent cells also behave like lenses and this effect is neglected in this approach. It is however suitable for calculations, when the optical ray propagates through areas where laminar flow is present.

2.2.2 ABCD matrices

This method, also known as Ray tracing matrices, also relies on geometrical optics. It views turbulent cells as optical elements and links each cell to a certain matrix. Depending on how the turbulent cell is described, several types of matrices may be used [1].

$$\begin{pmatrix} A & B \\ C & D \end{pmatrix} = \begin{pmatrix} 1 & t \\ 0 & 1 \end{pmatrix} \quad (2.20)$$

Eq. (2.20) represents a matrix describing the same situation as is shown in Fig. 4, a medium with a constant refractive index, where t is the thickness of the cell.

$$\begin{pmatrix} A & B \\ C & D \end{pmatrix} = \begin{pmatrix} 1 & 0 \\ \frac{n_1 - n_2}{R_1 n_2} & \frac{n_1}{n_2} \end{pmatrix} \quad (2.21)$$

Eq. (2.21) represents a matrix describing a lens, with a curvature radius R_l and a refractive index n_2 . It accounts for an incident wave passing through the interface between the lens and the medium before it with a refractive index n_2 .

Those two matrices can be combined, to chain the optical elements together and hence easily include all the said effects of the turbulent cell together, as in Eq. (2.22)

$$\begin{pmatrix} A & B \\ C & D \end{pmatrix} = \begin{pmatrix} 1 & 0 \\ \frac{n_2 - n_1}{R_2 n_1} & \frac{n_2}{n_1} \end{pmatrix} \cdot \begin{pmatrix} 1 & t \\ 0 & 1 \end{pmatrix} \cdot \begin{pmatrix} 1 & 0 \\ \frac{n_1 - n_2}{R_1 n_2} & \frac{n_1}{n_2} \end{pmatrix}, \quad (2.22)$$

where the matrices represent, from left to right, lens at the interface $n_1|n_2$, inside of the cell with a constant refractive index n_2 and thickness t , and the lens at the interface $n_2|n_1$.

With the knowledge of the ABCD matrix, to determine the deflection of the optical ray, leaving the turbulent cell, it is enough to multiply ABCD matrix by a column vector, with a distance of the source from the primary optical axis at the first position and an angle at which the optical ray is passing the interface, which is called the deflection vector, just like in Eq. (2.23)

$$\begin{pmatrix} x_2 \\ \theta_2 \end{pmatrix} = \begin{pmatrix} A & B \\ C & D \end{pmatrix} \cdot \begin{pmatrix} x_1 \\ \theta_1 \end{pmatrix}, \quad (2.23)$$

where x_1, x_2 are the distances from the optical axis of the system at the end of the turbulent cell (x_2) and at the beginning of the turbulent cell (x_1), θ_1 and θ_2 are the angles of divergence of the optical ray from the optical axis at the end of the turbulent cell (θ_2) and at the beginning of the turbulent cell (θ_1) and A, B, C and D are the parameters of the ABCD ray-tracing matrix. This situation is illustrated in Fig. 5.

As this method is based on paraxial approximation, the presence of paraxial rays is a requirement for using this method with suitable precision, which means that condition for the input angle θ_1 must be met [7], as is shown in Eq. (2.24)

$$\sin(\theta_1) \cong \theta_1 \quad (2.24)$$

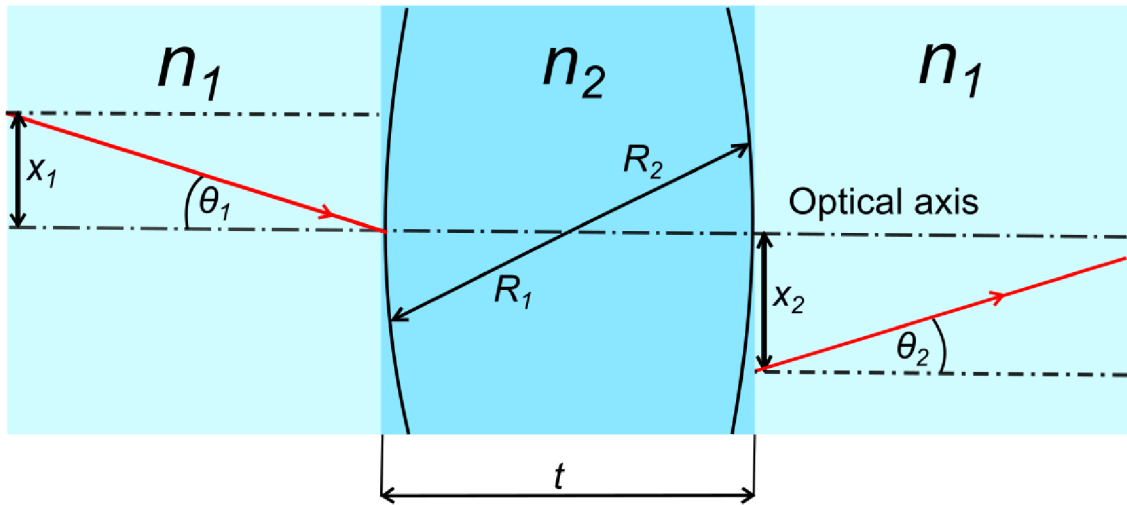


Figure 5: Calculation of the turbulent beam deflection using Ray tracing matrices.

More optical elements could be chained together, simply by multiplying them, in a way that the matrix representing the first element in the chain must be at the rightmost side of the equation, because the order of operation in matrix multiplication is crucial. Turbulent underwater space can be divided into N turbulent cells, where each cell has its own refractive index n_n , thickness t_n , curvature radii $R_{n,1}, R_{n,2}$ and the individual cells are at the distance l away from each other as can be seen in the Fig. 6.

To calculate the beam deflection by the whole cascade of turbulent cells, it is first needed to determine the distance x_{1N} , which is the initial deflection of the optical beam

caused by the angle of divergence of the optical source. This distance can be calculated using trigonometric functions, as in Eq. (2.25)

$$x_{IN} = l_{TX} \cdot \text{tg}(\theta_{IN}), \quad (2.25)$$

where l_{TX} is the distance between the transmitter and the first turbulent cell and θ_{IN} is the angle of divergence of the transmitter.

The total beam deflection after the passage through the whole turbulent space can be calculated according to the Eq. (2.26) [1]

$$\overrightarrow{X_{OUT}} = L_{RX} \cdot T_n \cdot \dots \cdot L_2 \cdot T_2 \cdot L_1 \cdot T_1 \cdot \overrightarrow{X_{IN}}, \quad (2.26)$$

where $\overrightarrow{X_{OUT}} = \begin{pmatrix} x_{out} \\ \theta_{out} \end{pmatrix}$ is the deflection vector at the output of the turbulent cell and $\overrightarrow{X_{IN}} = \begin{pmatrix} x_{in} \\ \theta_{in} \end{pmatrix}$ the deflection vector at the input of the turbulent cell, L_n is the ABCD matrix of the inter-turbulent space, as in Eq. (2.20) and T_n is the ABCD matrix of a turbulent cell, as in Eq. (2.22).

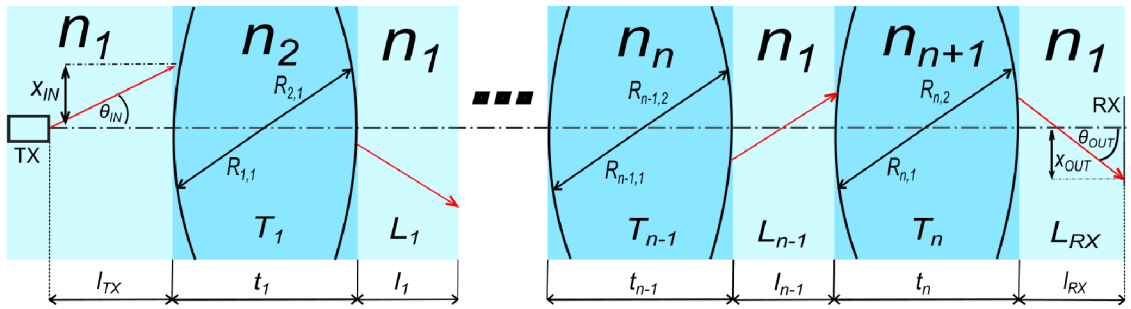


Figure 6: Illustrative model of N turbulent cells chained together representing a turbulent space.

As water is an anisotropic medium, the refractive indexes of each turbulent cell are different in x and y axis, which means that to get the total spatial deflection of the optical beam, deflection vectors in both axes $\overrightarrow{x_{OUT}} = \begin{pmatrix} x_{out} \\ \theta_{out} \end{pmatrix}$ and $\overrightarrow{y_{OUT}} = \begin{pmatrix} y_{out} \\ \Phi_{out} \end{pmatrix}$ need to be calculated separately and then their spatial coordinates need to be summed together to get the resulting deflection vector $\vec{v} = \begin{pmatrix} x_{out} \\ y_{out} \end{pmatrix}$, as is illustrated in Fig. 7. In this image, the beam is propagating from the black box (representing the transmitter) on the left side, through a turbulent space represented by four turbulent spherical cells, into the receiving lens, represented by a black box on the right side. In this scenario, no power is received by the used receiver, as the beam is completely deflected by the turbulent space, the deflection vector is depicted by an orange arrow. The optical axis of the system is represented by the pink line connecting the transmitter and the receiver.

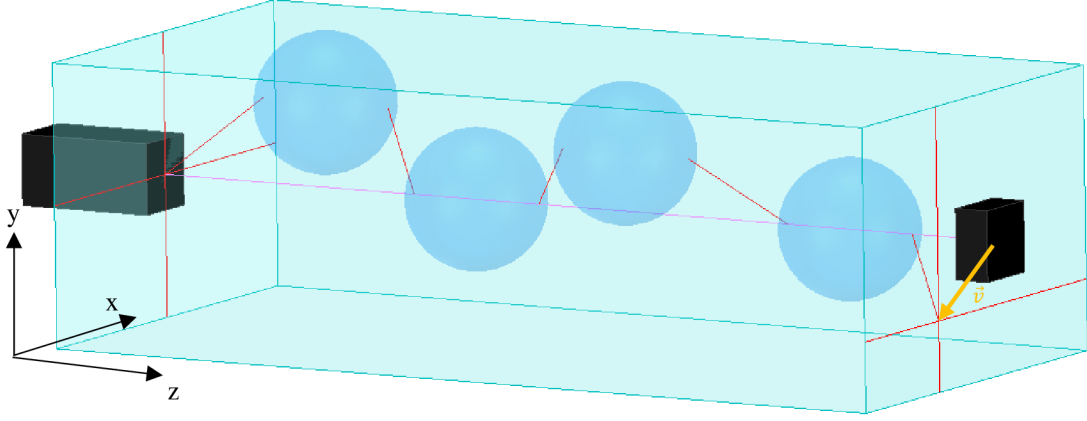


Figure 7: Visualization of the beam deflection while propagating through a 3D turbulent space.

In applications, where duplex communication is desired, the question of reciprocity of the turbulent system comes into consideration. Unfortunately, the system of turbulent cells is not reciprocal, because the scattering properties of turbulence are asymmetric with respect to the reversal of the propagation direction. This is caused by the fact that turbulence is a random process, and the random phase shifts that are introduced by the turbulence are not reversible [8]. The reciprocity of the underwater turbulent space is further analysed in [9]. To analyse the deflection of the optical beam propagating in the opposite direction, one needs to reverse the order of the matrices in the matrix multiplication, as in Eq. (2.27)

$$\overrightarrow{X_{OUT}} = L_{RX} \cdot T_1 \cdot \dots \cdot L_1 \cdot T_{n-1} \cdot L_{n-1} \cdot T_n \cdot \overrightarrow{X_{IN}}. \quad (2.27)$$

2.2.3 Received power calculation

To calculate the power received by the receiving lens at the receiver it is necessary to first determine the distance by which the beam is deflected from the optical axis of the system, after propagating through the system of turbulent cells. The method used depends on the direction of communication. If the aim is to communicate vertically, for example between the ocean bed and a buoy on the surface of the sea, the water flow will be mostly laminar and so the easier method, based on Snell's law, Eq. (2.19), can be used or the matrix approach may be used as well, by representing the laminar flow by matrix from Eq. (2.20). If the communication is to happen in a horizontal direction, for example between two submarines, then the Ray-tracing approach has to be used, as the water flow will be mostly turbulent in this direction and the effect of the turbulent lenses must be taken into account to obtain reliable results.

Once the resulting deflection vector is known, the received power by the receiving lens, if we account for a gaussian beam profile of the transmitted optical beam, can be calculated, as in Eq. (2.28)

$$P_0(z) = \int_{y_1}^{y_2} \int_{x_1}^{x_2} I_0 \cdot \left[\frac{w_0}{w(z)} \right]^2 \cdot e^{-\frac{x^2+y^2}{w^2(z)}} dx dy, \quad (2.28)$$

where I_0 is the amplitude of the beams' optical intensity, w_0 is the waist radius of the beam, $w(z)$ is the radius of the beam at the distance z from the transmitter, x and y are spatial coordinates. No primitive function exists for the operand e^{x^2} which means, that the integral in Eq. (2.28) cannot be evaluated analytically. It can either be solved numerically, or using Taylor's expansion, which will be this case. Using Taylor's expansion, the above-mentioned operand can be rewritten as in Eq. (2.29)

$$e^{x^2} \cong 1 + x^2 + \frac{x^4}{2} + \frac{x^6}{6} + \frac{x^8}{24} + O(x^9) = \sum_{k=0}^{\infty} \frac{(x^2)^k}{k!}, \quad (2.29)$$

where $O(x^9)$ is the Big O notation, from the Landau operators. After doing this substitution, the integral can be evaluated analytically to obtain the following formula for the power received by the receiving lens P_0

$$P_0(z) = A(z) \cdot \left[\operatorname{erf}\left(\frac{\sqrt{2}}{w(z)} \cdot x_2\right) - \operatorname{erf}\left(\frac{\sqrt{2}}{w(z)} \cdot x_1\right) \right] \cdot \left[\operatorname{erf}\left(\frac{\sqrt{2}}{w(z)} \cdot y_2\right) - \operatorname{erf}\left(\frac{\sqrt{2}}{w(z)} \cdot y_1\right) \right], \quad (2.30)$$

where $w(z)$ is the beam radius at the distance z from the transmitter, $x_{2,1}$ and $y_{2,1}$ are the coordinates of the receiving lens, deflected by the turbulence in x and y axis as is shown in Fig. 8 and 9, erf is the error function, defined as in Eq. (2.31) and $A(z)$ is a distance dependent coefficient defined to improve readability of the Eq. (2.30) and is defined as in Eq. (2.32)

$$\operatorname{erf}(x) = \frac{2}{\sqrt{\pi}} \int_0^x e^{-t^2} dt, \quad (2.31)$$

$$A(z) = \frac{\pi}{8} \cdot w^2(z) \cdot I_0 \cdot \left[\frac{w_0}{w(z)} \right]^2, \quad (2.32)$$

where $w(z)$ is the beam radius at the distance z from the transmitter, I_0 is the amplitude of the optical intensity and w_0 is the waist radius of the beam. The beam radius can be computed as follows in Eq. (2.33)

$$w(z) = w_0 \left[1 + \left(\frac{z}{z_0} \right)^2 \right]^{\frac{1}{2}}, \quad (2.33)$$

where z_0 is the Rayleigh length defined as follows in Eq. (2.34)

$$z_0 = \frac{\pi \cdot w_0^2}{\lambda}. \quad (2.34)$$

The coordinates of the receiving lens $x_{1,2}$ and $y_{1,2}$ can be calculated from the dimensions of the receiving lens, approximated in this case as a rectangle, of side length d and the deflection vector, as in Eq. (2.35) and (2.36)

$$y_{1,2} = \pm \frac{d}{2} + y_{out}, \quad (2.35)$$

$$x_{1,2} = \pm \frac{d}{2} + x_{out}, \quad (2.36)$$

where y_{out}, x_{out} are the y and x coordinates of the deflection vector \vec{v} . If a circular receiving lens of radius r is to be used, it can be approximated in the calculations by a rectangle of side length d with the same area. The equivalent side length d_{eq} can be calculated as in Eq. (2.37)

$$\begin{aligned} S_o &= S_{\blacksquare}, \\ \pi \cdot r^2 &= d^2, \\ d_{eq} &= r \cdot \sqrt{\pi}. \end{aligned} \quad (2.37)$$

If this simplification is not suitable for the given situation, more precise approach can be used. The integral from Eq. (2.28) can be transformed into polar coordinates, as in Eq. (2.38)

$$P = \int_0^{2\pi} \int_0^a A(z) \cdot r \cdot e^{-2 \frac{(r \cdot \cos \theta + x_{out})^2 + (r \cdot \sin \theta + y_{out})^2}{w^2(z)}} dr d\theta, \quad (2.38)$$

where r is the radius and θ is the angle of the polar coordinates and a [m] is the radius of the receiving lens. For this method to be applicable, as the gaussian beam is deflected from the origin by the deflection vector, it needs to be considered in the calculations, by subtracting the coordinates of the deflection vector from the coordinates of the gaussian beam. This form of the integral cannot be solved analytically, as the integral is transcendent, thus a numerical solution needs to be found.

The power integrated by the receiving lens further needs to be multiplied by the attenuation coefficient to account for absorption and scattering, as in Eq. (2.14).

To calculate the incident angle ψ at which the optical beam leaves the turbulence, the following formula derived from trigonometric functions in Eq. (2.39) can be used

$$\psi = \arctg\left(\frac{y_{out} \cdot \text{tg}(\phi)}{\|\vec{v}\|}\right) \text{ or } \psi = \arctg\left(\frac{x_{out} \cdot \text{tg}(\theta)}{\|\vec{v}\|}\right), \quad (2.39)$$

where x_{out}, y_{out} is the deflection at the output of the turbulence in the x and y axis respectively, θ and ϕ are the angles at which the optical beam leaves the turbulence in x and y axis respectively and $||\vec{v}||$ is the length of the resulting deflection vector calculated as in Eq. (2.40)

$$||\vec{v}|| = \sqrt{x_{out}^2 + y_{out}^2}, \quad (2.40)$$

this situation is visualised in the Fig. 8.

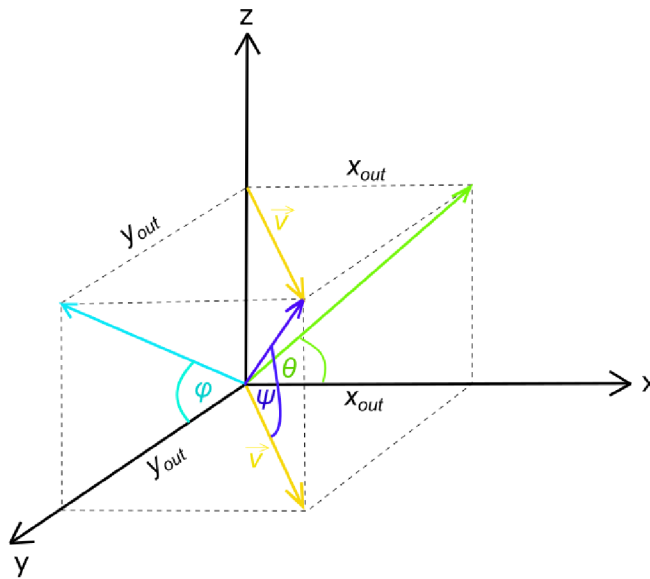


Figure 8: Visualization of the incidence angle ψ calculation from calculated deflection vectors in x and y axes, z is the optical axis of the system.

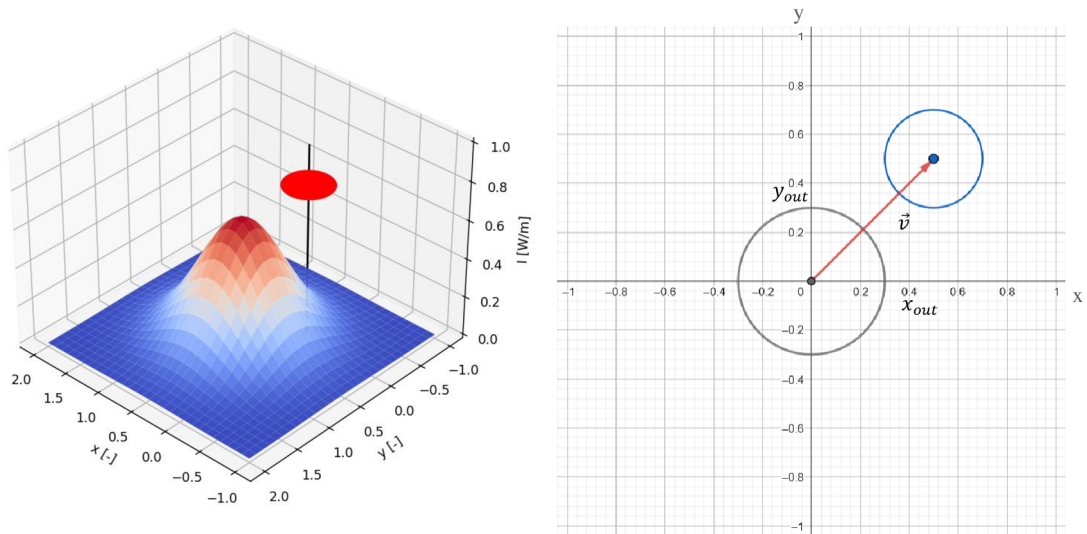


Figure 9: 3D representation of the beam deflection, red circle is the receiving lens, black line is the optical axis and the contour is the gaussian beam profile (left side), XY cut in height $z = 0,5$ of the graph on the left side, showing beam's deflection vector \vec{v} (red) and the gaussian beam deflection (blue circle), the optical axis points outwards from point $[0, 0]$ (right side).

2.3 Solar radiation

To determine the amount of solar noise in a particular depth under water the same procedure as for the calculation of attenuation of the optical beam can be used. It depends on the concentration of chlorophyll. Chlorophyll concentration profile $C_c(z)$ needs to be calculated, according to Eq. (1.8), from which the attenuation profile can be calculated, as in Eq. (1.5) and after integrating it from the surface level to the depth, where the receiver is located, the total attenuation L_{sol} of the solar radiation can be determined, as in Eq. (2.40)

$$L_{sol} = \int_{z=0}^{z_{rec}} C_c(z) dz, \quad (2.40)$$

where z_{rec} is the depth at which the receiver is located, $z = 0$ is the surface level of the body of water and $C_c(z)$ is the depth dependent attenuation profile, as in Eq. (1.8).

2.4 Optical link budget

To ensure reliable communication between the transmitter and the receiver, the optical power available at the receiving side, must be within the limits that the receiver can work with. This situation is depicted in the Fig. 10. On the vertical optical power axis are plotted important power levels of the system. P_{sat} is the saturation power level, it's the maximum power level that can be processed by the receiver, P_{min} is the minimum desired power level to be present at the receiver for acceptable *bit error rate (BER)* of the received data stream and P_{noise} is the background noise power level below which no signal can be received. The difference between minimal and noise level is called *minimal signal to noise ratio* SNR_{min} . In general, it can be said, that the greater the SNR , the lower the BER and the better the performance of the system [6].

As the signal propagates through the optical link, it gets both amplified and attenuated. Those changes can be seen in the Fig. 10. L_{TX} is the attenuation at the receiver, G_{TX} is the gain of the transmitting lens, L_{CH} is the channel attenuation, G_{RX} is the gain of the receiving lens and L_{RX} is the attenuation at the transmitter. The difference between the power available at the receiver and the minimal desired power level at the received is called the *power margin* ρ . It should always be greater than zero, to account for possible increase of attenuation in the communication channel, because of unpredictable reasons like an increase in the intensity of the turbulence [6].

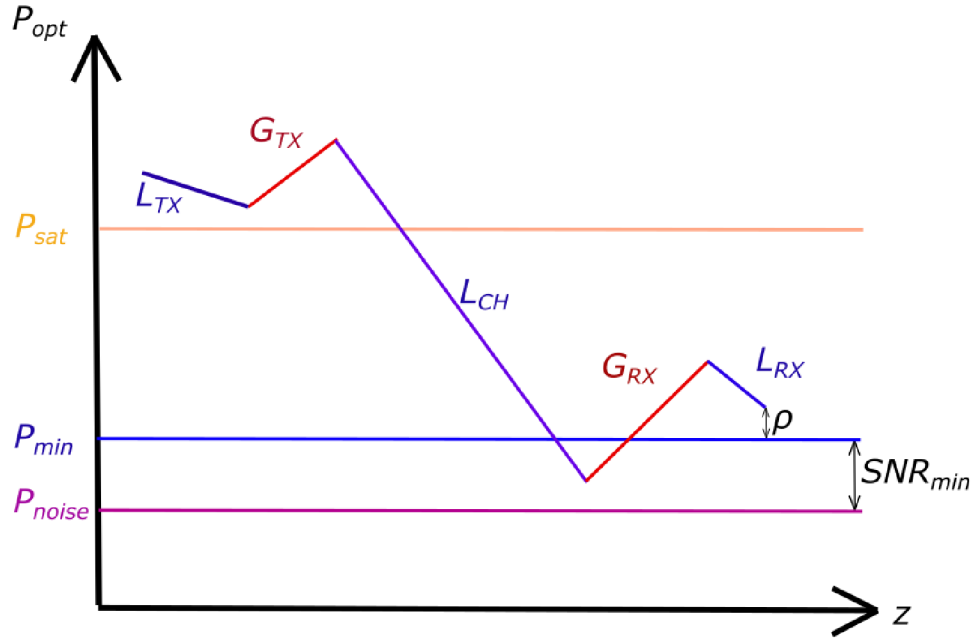


Figure 10: Visualization of optical link budget calculation, z is the distance from the transmitter.

2.5 Modulation scheme

Before the data can be sent via the designed optical link, they first need to be modulated on the carrier. Various digital modulations can be used for this task, differing in achievable bitrate, required modulation bandwidth of the transmitter, spectral efficiency of the modulation and the required SNR for desired BER . [28]

2.5.1 On-off keying (OOK)

This is the simplest method of data modulation, based upon the Amplitude Shift Keying (ASK). When the carrier wave is turned on, logical ‘1’ is being transmitted, logical ‘0’ is represented by the carrier wave being turned off.

Two variants of this modulation are used – return to zero on-off keying (RZ-OOK) and non-return to zero on-off keying (NRZ-OOK). The former type, as the name suggest, returns, after transmitting a bit, to the off state, whereas the latter stays in the on state, until changed by the transmission of another bit.

Maximum achievable bitrate of NRZ-OOK is given as

$$v_i = BW, \quad (2.41)$$

where BW is the modulation bandwidth of the optical transmitter. Maximum achievable bitrate of RZ-OOK is given as

$$v_i = \frac{1}{2}BW. \quad (2.42)$$

2.5.2 Pulse amplitude modulation (PAM)

This is another form of ASK. Multiple bits are transmitted at once, the number of bits transmitted depends on the number of amplitude levels, the modulation uses. This modulation is also referred to as M-PAM, where M stands for the number of amplitudes,

the modulation uses. M is a power of two and to determine the number of bits transmitted at once L , the formula (2.43) can be used

$$L = \log_2 M . \quad (2.43)$$

The higher the number of states, the higher the SNR needs to be to achieve desired BER , but higher bitrates can be achieved. [28]

Maximum achievable bitrate of M-PAM is given by Eq. (2.44)

$$v_i = \log_2 M \cdot BW . \quad (2.44)$$

2.5.3 Pulse position modulation (PPM)

This modulation encodes bites into the position of pulses. This modulation cannot transmit more than one data bit at a time, it is less susceptible to noise though, as the amplitude of the laser only has two states, just like OOK. It is possible to increase the bitrate by increasing the number of consecutive pulses, creating M-PPM modulation, where M has the same meaning as in the previously mentioned modulation. The higher the number of states the higher the modulation bandwidth of the transmitter needs to be.

The maximum achievable bitrate of M-PPM is given by formula (2.45)

$$v_i = BW \cdot \frac{\log_2 M}{M} . \quad (2.45)$$

The performance of all mentioned modulations, regarding the achievable BER for attained SNR is plotted in the Fig. 11. Modulation RZ-OOK has the same performance as 2-PAM and 2-PPM. [28]

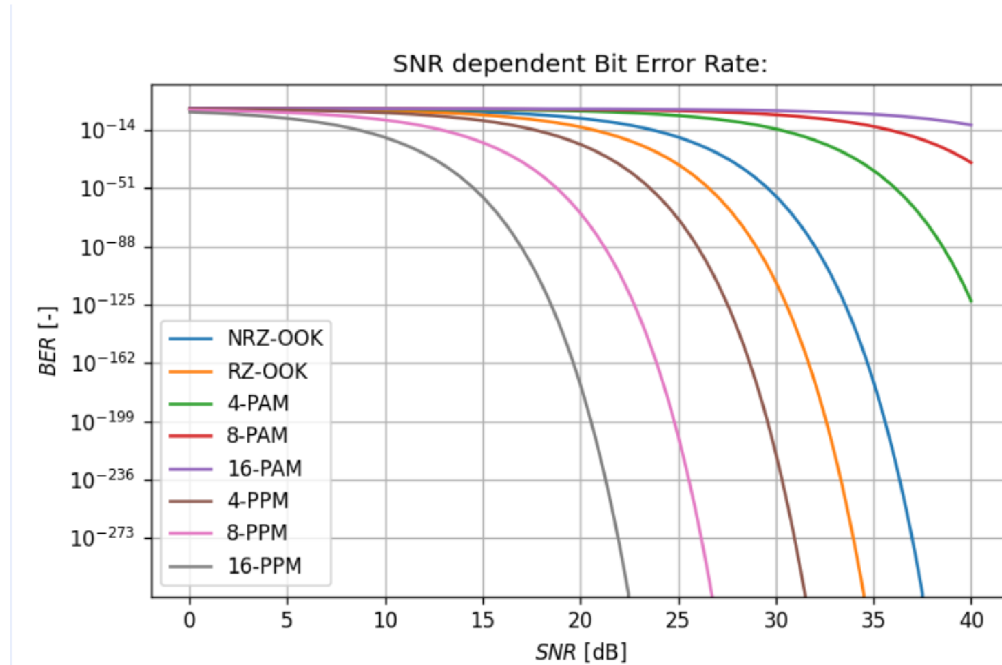


Figure 11: Achievable BER for attained SNR .

3. SOFTWARE IMPLEMENTATION

The above-mentioned procedures for calculating propagation of an optical ray through and underwater turbulent space have been implemented in Python, see files attached to the master's thesis. The flowchart of the algorithm for optical ray attenuation due to propagation through turbulence can be seen in Appendix A.

The generation of the parameters of the turbulent space is done in a stochastic manner. In the program, mean values of the parameters are defined, to which stochastic values from gaussian or lognormal distribution of given parameters are superimposed, which means that for each run of the algorithm, a different number of turbulent cells of different parameters is generated, simulating the dynamic nature of the turbulence. By adjusting the mean value and standard deviation of the gaussian distribution, the strength of the turbulence can be controlled.

3.1 Program description

Graphical user interface (*GUI*) of the program was created with the help of Python module named Tkinter. Title page of the program can be seen in the Fig. 12. Program functionalities can be invoked from the overhead menu, highlighted in the Fig. 12 by a red rectangle and its detail can be seen in the Fig. 13. In the program, database of optical components is present, transfer chain and transmission medium can be defined, appropriate signal modulation and optical wavelength can be determined and there is a window for displaying the results of the calculations. Individual functionalities shall be described in the following subchapters.

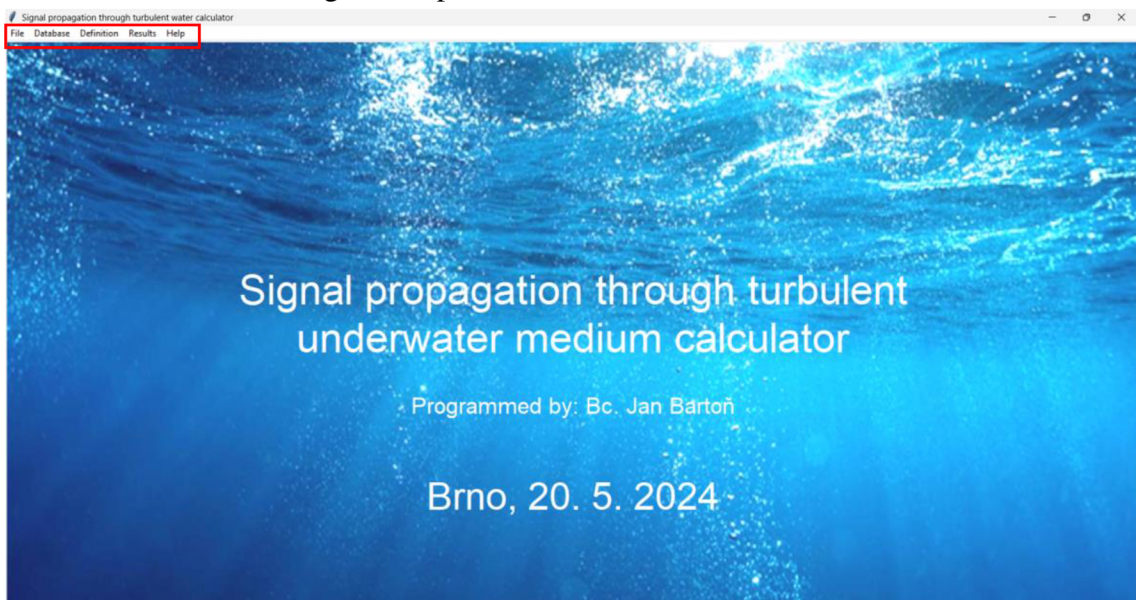


Figure 12: Title page of the program.

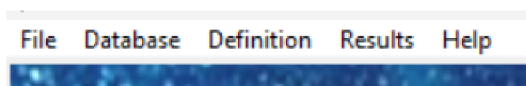


Figure 13: Detail of the overhead menu.

3.1.1 Database

Under the item “Database” in the overhead menu, database of individual optical components can be invoked. Among those components belong lenses, cover windows, detectors, optical filters and transmitters, as is illustrated in the Fig. 14.

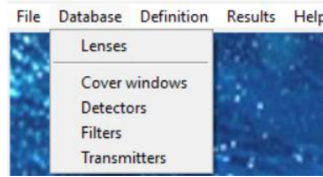


Figure 14: Menu item “database”.

Each component’s database contains predefined components, whose parameters can be modified according to the needs of the user and there is also a possibility to define new custom components to be included into the existing database.

3.1.1.1 Lenses

The functionalities of the database interface shall be demonstrated at the database of lenses, pictured in the Fig. 15.

Predefined lenses and their parameters can be viewed upon clicking on an item from the drop-down menu, marked in the Fig. 15 by a red rectangle. Preset parameters, that appear in the boxes below, can be modified by writing new values into corresponding boxes and confirming the changes by clicking on the button labelled as “Edit”, marked by a green box in this image.

New items can be added into database by first clicking on the button labelled as “Add lens”, in case of the database of lenses, highlighted in the Fig. 15 by a blue rectangle, and then name of the item and its parameters can be set by writing desired values into corresponding boxes. Items can be saved into the database by pressing the button labelled as “Enter”, marked by a pink rectangle in the Fig. 15.

Meaning of parameters of the lenses can be seen in the pictures below the database interface, marked by a yellow rectangle. Both images were taken from [26].



Figure 15: Database of lenses window.

3.1.1.2 Cover windows

The interface of the database of cover windows is pictured in the Fig. 13. The illustration image at the bottom of the Fig. 16 is taken from [26]. Diameter, attenuation and price of cover windows can be set.



Figure 16: Database of cover windows window.

3.1.1.3 Transmitters

The interface of the database of transmitters is pictured in the Fig. 17. The illustration image at the bottom of the Fig. 17 is taken from [26]. Angles at which the optical ray emitted from the transmitter diverges from the optical axis in both axes (see chapter 2.2.2 for more information), the output power of the laser, wavelength of the beam, its deviation, modulation bandwidth and the price of the transmitter can be defined.

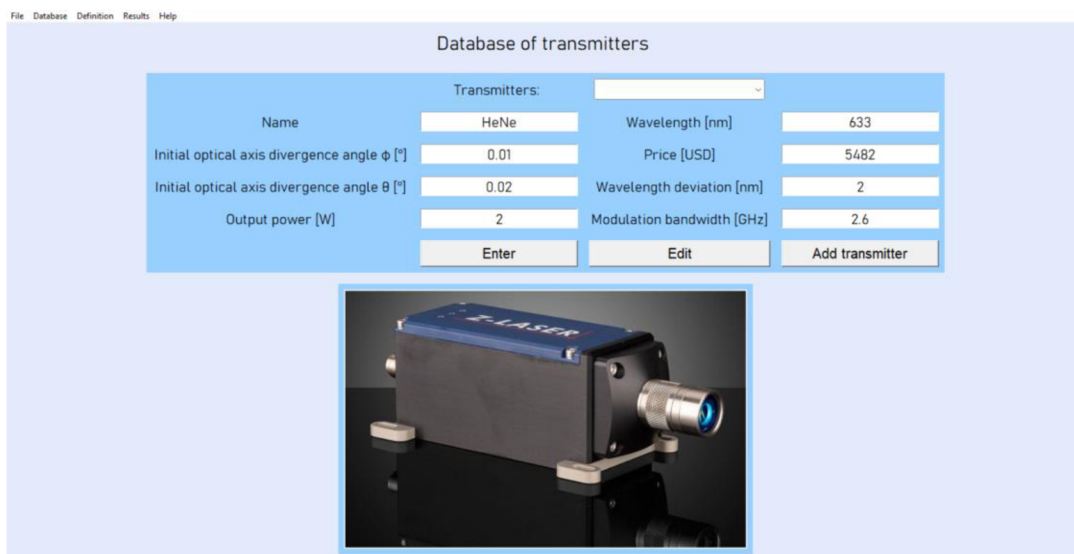


Figure 17: Database of transmitters window.

3.1.1.4 Filters

The interface of the database of filters is pictured in the Fig. 18. The illustration image at the bottom of the Fig. 18 is taken from [27]. Free spectral range, finesse, pass and stop wavelengths, insertion loss, resolution, cavity length, transmittance and the price of the filter can be defined.



Figure 18: Database of filters window.

3.1.1.5 Receivers

The interface of the database of receivers is pictured in the Fig. 19. The illustration image at the bottom of the Fig. 19 is taken from [27]. Detector area, SNR, minimal number of photons, saturation power, pass and stop wavelengths, quantum efficiency, responsivity and the price of the receiver can be set.

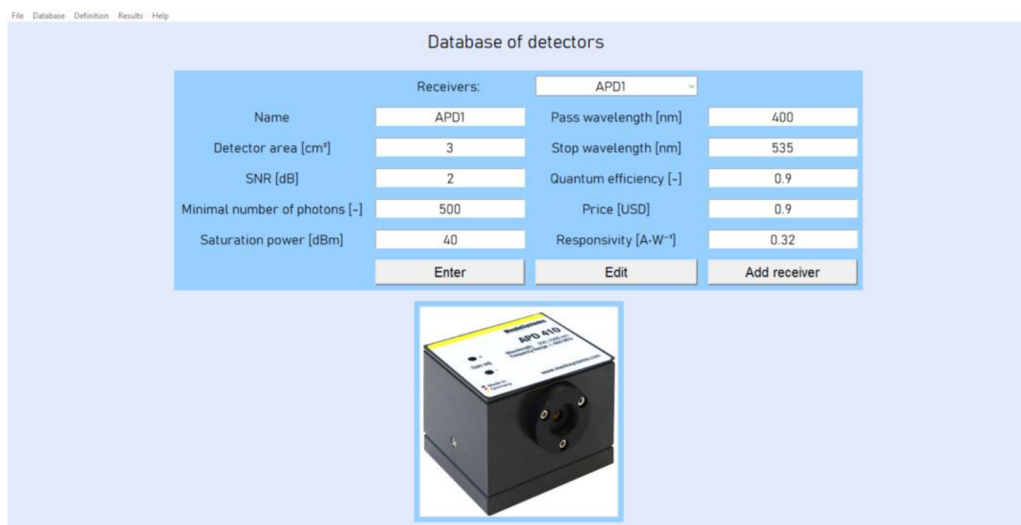


Figure 19: Database of receivers window.

3.1.2 Definition of environment

Under the item “Definition” in the overhead menu, the properties of the transmission medium can be defined. It consists of definition of the transfer chain and the transmission medium, of a tool to select an appropriate wavelength of the optical ray for the defined parameters of the environment and of a tool to choose a suitable modulation and calculate required Signal to Noise Ratio (*SNR*), as is depicted in the Fig. 20.

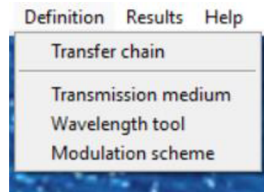


Figure 20: Menu item “Definition”.

3.1.2.1 Transfer chain definition

This window serves the purpose of selecting which components from the database shall be used in the optical transfer chain. Components can be selected from the drop-down menus, highlighted by a red rectangle in the Fig. 21. The transfer chain consists of a transmitter, transmitting lens, transmitter cover window, receiver cover window, receiving lens, an optical filter, whose usage is optional, depending on the amount of solar radiation (see chapter 2.3), and an optical receiver. Whether an optical filter shall be used is controlled by a checkbox, that is in the Fig. 21 highlighted by a green rectangle. Depending on the deflection of the optical ray from the optical axis of the link, offset can be added to the receiver to move it in the direction of the x and y axes from the optical axis in order to maximise the received power. The offset distances can be edited in the frames and saved by the button “Save data” highlighted in the Fig. 21, by a blue rectangle. The suggested offset can be determined from the window displaying results of the calculations (see chapter 3.1.3)

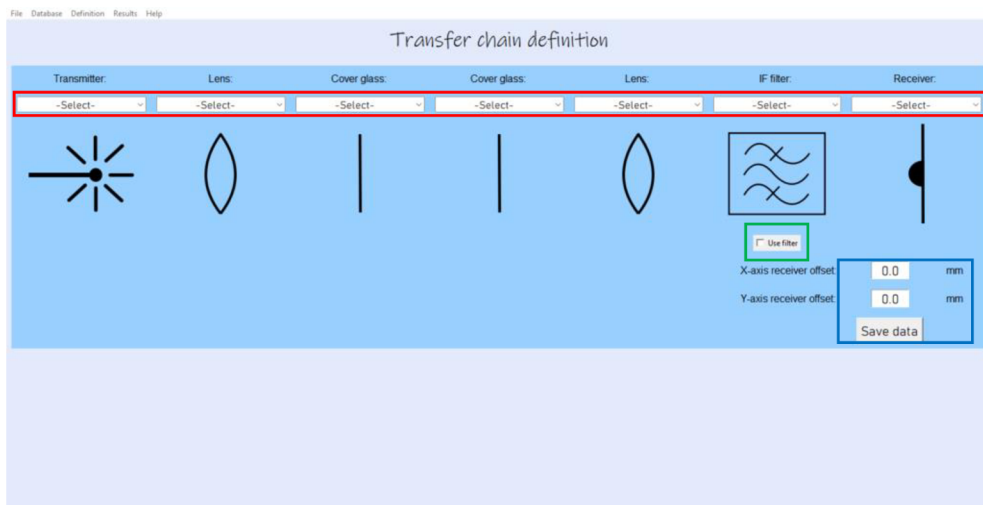


Figure 21: Transfer chain definition window.

3.1.2.2 Transmission medium definition

In this window, properties of the underwater turbulent space may be altered, namely the distance from the transmitter to the turbulence, the length of the turbulence and the distance from the turbulence to the receiver, the aforementioned parameters can be written into the corresponding boxes, in order going from left to right, highlighted in the Fig. 22 by a red rectangle, they are also marked directly in the program window, under the turbulence animation. It is also possible to define the depth under water, where the optical link will be situated, by writing the desired value into the box highlighted in the Fig. 22 by a green rectangle. Changes can be saved by the button labelled “Save data”, highlighted in the Fig. 22 by an orange rectangle. The direction of communication can be set, in either a horizontal or vertical direction by pressing a button highlighted in the Fig. 22 by a blue rectangle. Other parameters, that can be altered are the type of water and chlorophyll concentration, they can either be set manually by writing values into corresponding boxes highlighted in the Fig. 22 by a purple rectangle, or a built-in tool can be used to choose parameters valid for a specified geographical location. This tool can be invoked by pressing the button labelled “Choose from geographical position”, highlighted in the Fig. 22 by a yellow rectangle. Last thing that can be varied in this window is the strength of the turbulence, after pressing the button labelled as “Advanced turbulence settings”, highlighted by a pink rectangle in the Fig. 22.

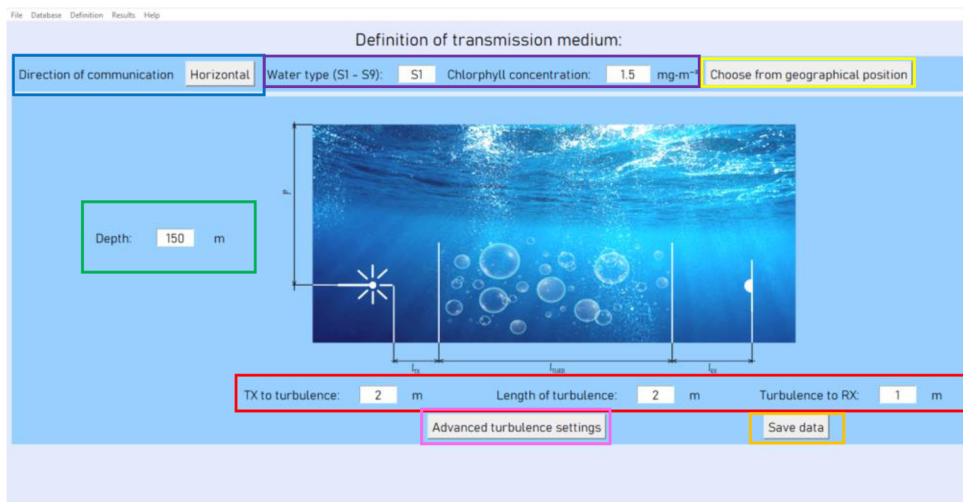


Figure 22: Transmission medium definition window.

The invoked window for choosing geographical location is depicted in the Fig. 23. The location can be selected by clicking at a desired location in a body of water. After doing the selection, a date and time selection window for the selected location will appear, where the user sets the desired time of operation of the link. From this information the solar irradiance at the surface of the selected body of water will be calculated. The date and time selection window is shown in the Fig. 24.

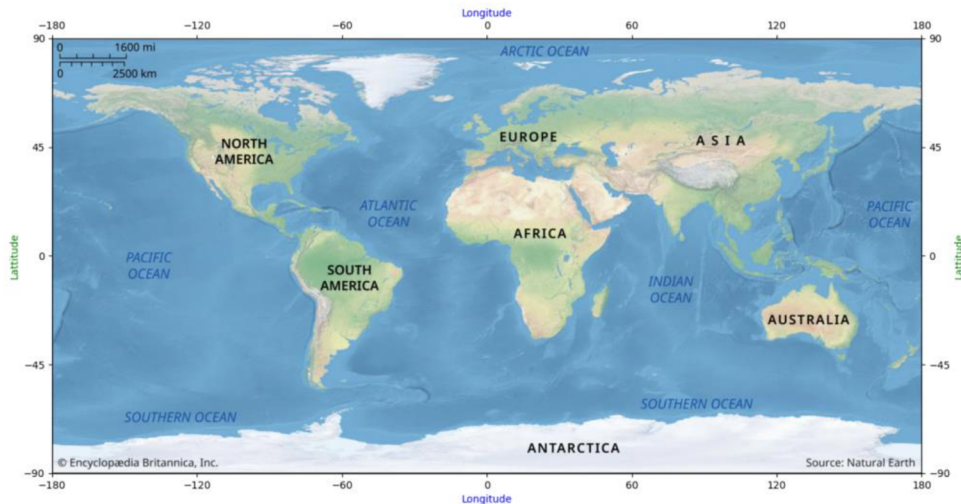


Figure 23: Choice of a geographical location window.

Figure 24: Date and time selection window.

The window for setting the turbulence strength, is shown in the Fig. 25. Parameters that can be varied using the corresponding sliders are curvature radius of the turbulent cells, the length of the cell, the interturbulent length and refractive indexes of turbulent cells, see section 2.2.2 for description of those parameters. An overview of individual parameters' meanings can also be invoked in the program, upon pressing button labelled as "Parameter description", highlighted in the Fig. 25 by a red rectangle. This description window is shown in the Fig. 26. As the turbulent cells within turbulence are generated in a stochastic manner, its parameters can be influenced by adjusting mean values and standard deviations of the distribution by which the individual parameters are described. User can choose between normal and lognormal distributions. After the selection is complete, changes need to be saved by pressing button labelled as "Save data", highlighted by a green rectangle in the Fig. 25.

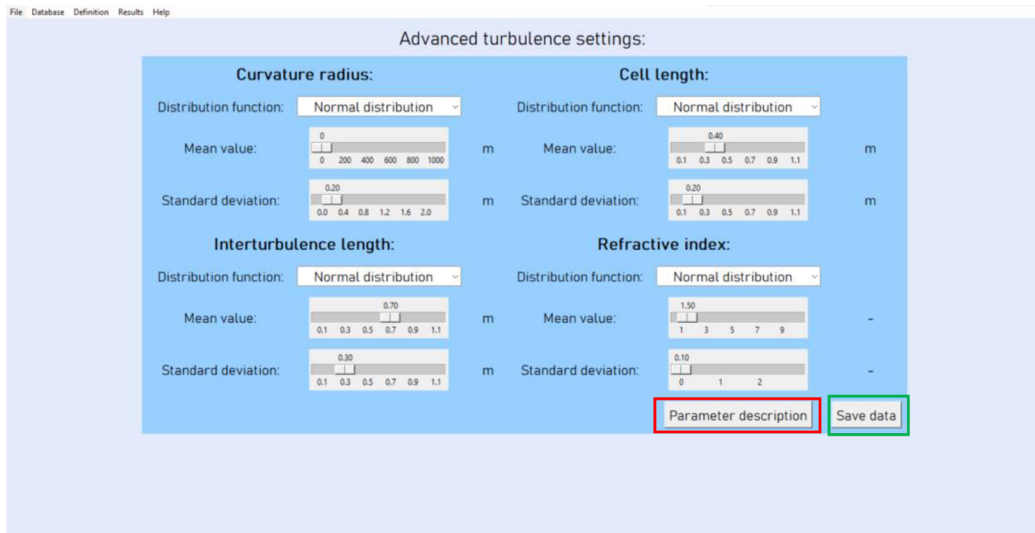


Figure 25: Turbulence strength settings window.

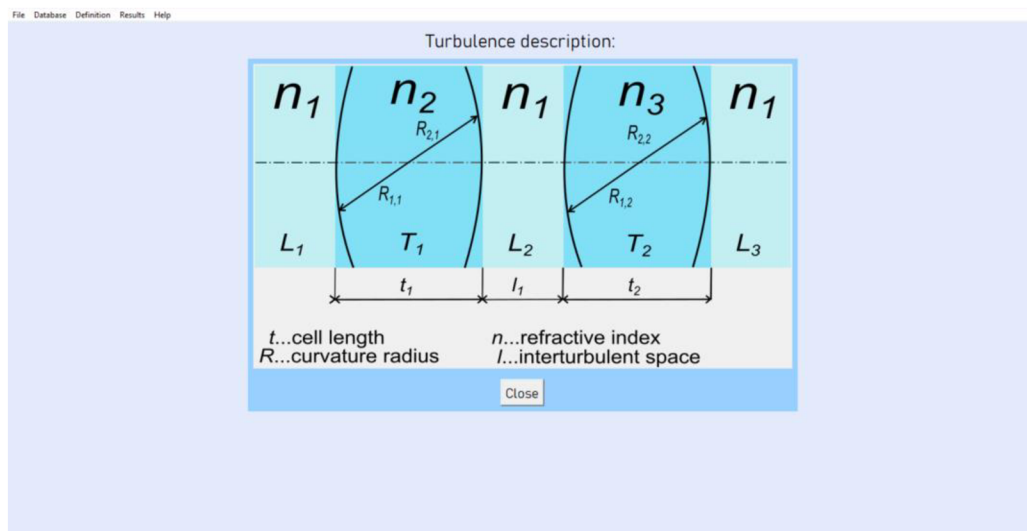


Figure 26: Description of turbulent parameters window.

3.1.2.3 Wavelength tool

After the parameters of the underwater transmission medium have been defined, the wavelength tool can be used to determine the optimal wavelength of the optical beam to achieve the minimal possible attenuation by medium. This window is depicted in the Fig. 27. There are two graphs in this window.

On the left side is a graph, showing wavelength dependent attenuation coefficients of various factors influencing the attenuation of the underwater medium, for the given concentration of chlorophyll (for detailed description see chapter 2.11). From this graph the optimal wavelength, at which the sum of all individual attenuations is the smallest is determined, marked by a purple vertical line in this graph and is also displayed below the graph, in the Fig. 27 highlighted by a red rectangle.

On the right side of the window is a graph showing a depth dependent chlorophyll concentration profile for the given water type.

There is also a possibility to switch the graphs to 3D view, by pressing the buttons labelled as “Switch to 3D”, highlighted in the Fig. 27 by a green rectangle. This situation is illustrated in the Fig. 28. In this setting, the graph on the left side shows the sum of all wavelength-dependent attenuation coefficients for all the most common chlorophyll concentrations at once and the graph on the right side show the depth dependent chlorophyll concentration profile for all possible types of water at once. Both of the graphs are interactive, which means that the user can rotate it around to be able to easier inspect them.

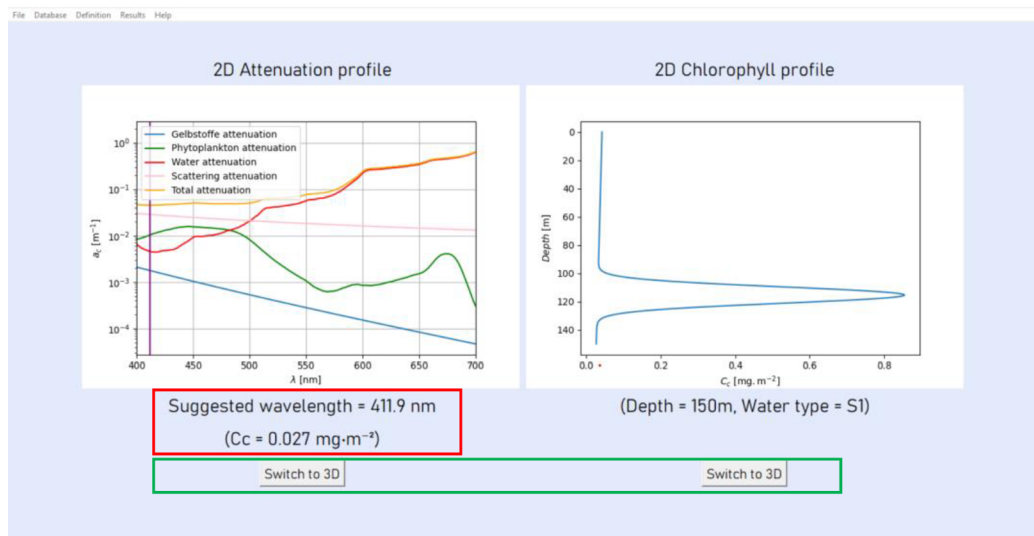


Figure 27: Wavelength tool window showing 2D graphs.

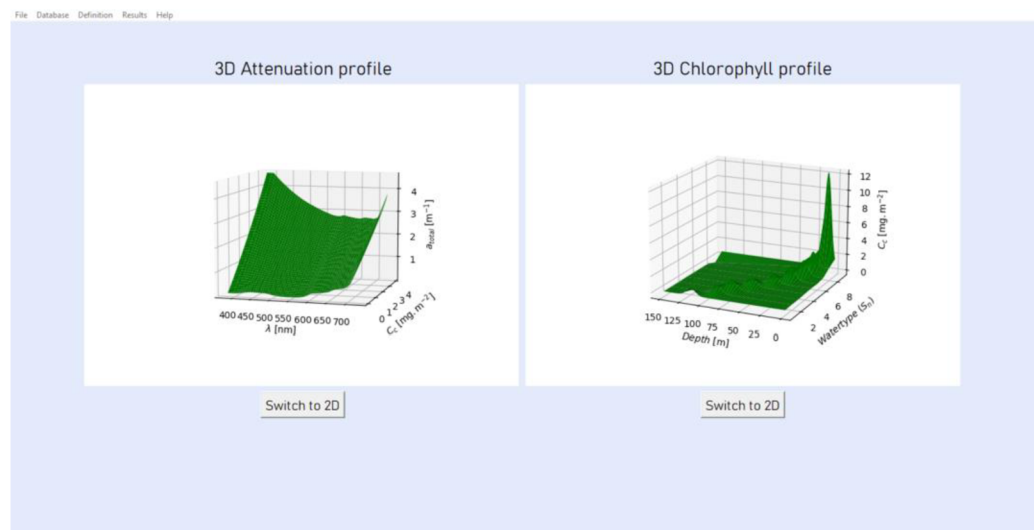


Figure 28: Wavelength tool window showing 3D graphs.

3.1.2.4 Modulation scheme selection

The last thing, the user needs to take care of, before the calculations can be initiated is the selection of an appropriate modulation scheme, according to which the data will be transmitted. This window is depicted in the Fig. 29.

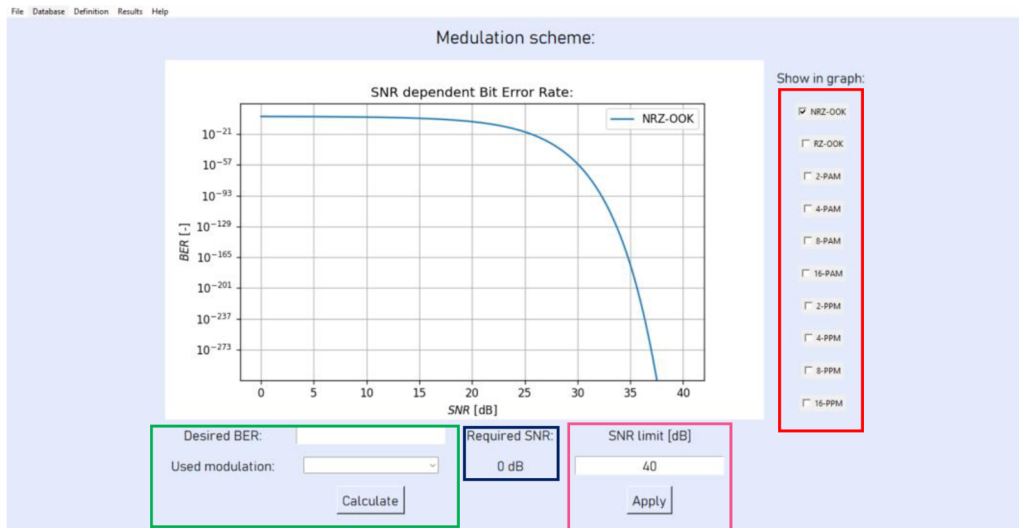


Figure 29: Modulation scheme selection window.

In this window, there is a graph plotting dependence of *Bit Error Rate (BER)* on *Signal to Noise Ratio (SNR)* for selected modulations. In the program, the most commonly used modulations are implemented but it can be easily extended by other modulations by a simple modification of the code. The limit of the x (*SNR*) axis can be modified by changing the value in the box under the title “SNR limit” and then confirming the change by the button labelled as “Apply” to make the graph as easily readable for the user as possible. This section is marked in the Fig. 29 by a pink rectangle.

To determine the required *SNR* for the desired *BER*, the user can either select the modulation that shall be used for the data encoding from the column on the right, highlighted in the Fig. 29 by a red rectangle, and then manually determining the value off the plotted graph, or the desired *BER* can be written into the box under the graph, along with setting the modulation to be used from the drop-down menu underneath it and pressing the button labelled as “Calculate”. This section is highlighted in the Fig. 29 by a green rectangle. The required *SNR* is then automatically calculated by the program and displayed in the section highlighted in the Fig. 29 by a blue rectangle.

3.1.3 Results

Under the item “Results” in the overhead menu, the calculations can be initiated upon pressing the “Perform calculations” submenu item, as is illustrated in the Fig. 30.

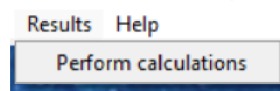


Figure 30: Menu item “Results”.

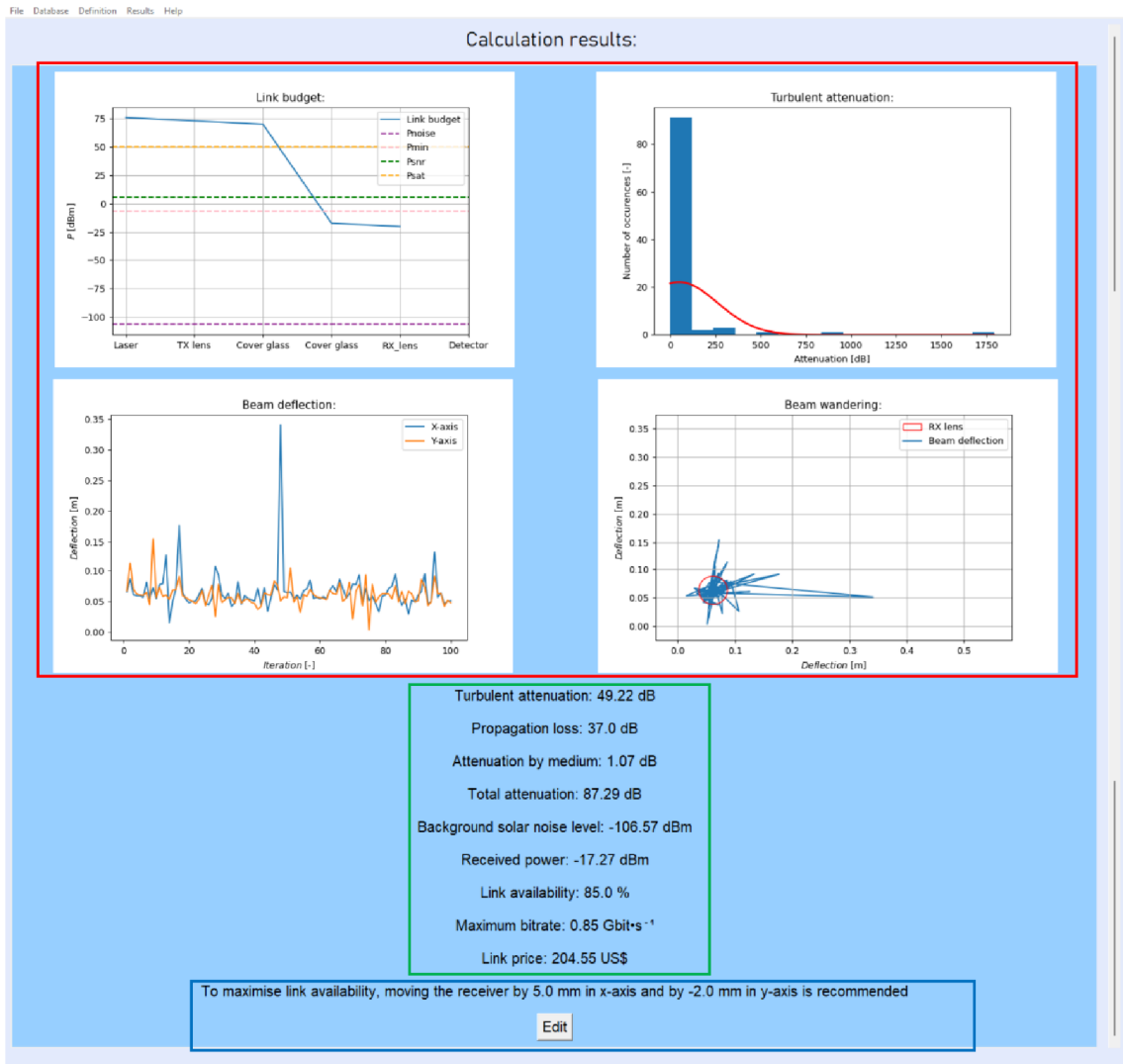


Figure 31: Results of the calculations window.

A window with results of example calculations is shown in Fig. 31. It consists of four graphs, a summary of mean values and a recommendation on how to improve link availability and a button labelled as “Edit” for executing the recommendation, marked in the Fig. 31 by a red, green and a blue rectangle respectively.

In the first graph, located in the northwest corner of Fig. 31, a calculated link budget is displayed, more information about link budget can be found in section 2.4.

In the second graph, located in the northeast corner of Fig. 31, a histogram, showing calculated turbulent attenuations for a given number of runs of the computation algorithm, set explicitly to one thousand, is plotted. There is also a red curve, representing theoretical normal distribution with mean value and standard deviation computed from the distribution of calculated turbulent attenuations, allowing the user to determine whether the turbulent attenuation changes according to normal distribution.

In the third graph, located in the southwest corner of Fig. 31, beam deflections in x (blue curve) and y axis (orange curve) is plotted, visualising how the deflection distance in each axis changes with each run of the algorithm.

In the fourth graph, located in the southeast corner of Fig. 31, beam wandering is plotted. In the given offset from the optical axis is the centre of a red circle representing the receiving lens and the blue curve represents the beam wandering, in which positions the centre of the transmitted beam was located at each run of the algorithm. From this graph, the optimal offset distance of the receiving lens from the optical axis can be determined.

Underneath the graphs in the Fig. 31, mean values of link parameters, calculated from all runs of the algorithm, are shown. Those parameters include turbulent attenuation, geometrical attenuation (propagation loss), attenuation by medium and the total attenuation, which is the sum of those three attenuations, and it also counts with the attenuation of used optical components, followed by the calculated noise level (only solar noise is taken into account), link availability, maximum bitrate and the resulting price of the transfer chain. The last information available to the user is a recommendation on how to improve the availability of the link. If the received power of the signal is below the calculated solar noise level, usage of a filter will be recommended and if the middle of the receiver is not in the optimal offset distance from the optical axis, improvement will be suggested.

3.1.4 Information about the program

Under the item “Help” in the overhead menu, information about the program can be displayed upon pressing the “About” submenu item, as is depicted in the Fig. 32. The invoked menu is shown in the Fig. 33.

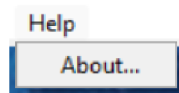


Figure 32: Menu item "Help".

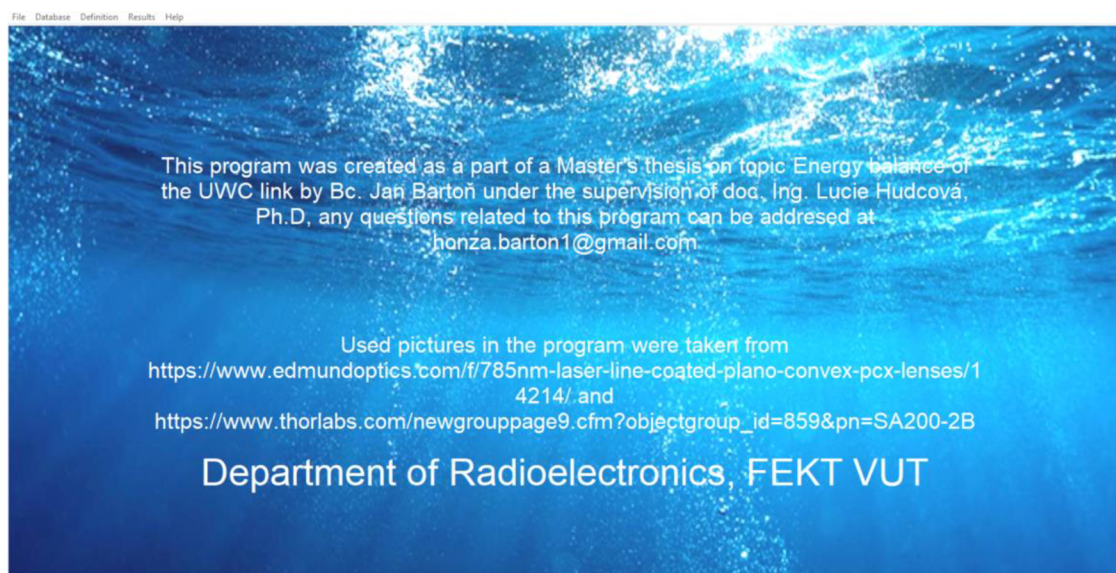


Figure 33: Window with information about the program..

3.1.5 Suggested procedure for link design

The following order of operations should be respected to solve the task of designing a wireless optical underwater link. The first thing that needs to be done, is to define the transmission medium (see chapter 3.1.2.2), to match the conditions given by the assignment.

After all of the parameters of the transmission medium have been set, the optimal wavelength of the optical beam should be chosen. For this task, the wavelength tool can be utilised (see chapter 3.1.2.3). When the wavelength is known a transmitter can be chosen. This minimises the attenuation by medium.

Next step is to choose the optimal modulation used for the communication. The modulation scheme selection tool is used for this task. From the knowledge of the desired speed of data transfer and the modulation bandwidth of the chosen transmitter, the best modulation to be used can be determined (see chapter 2.5). The subsequent step is to write the desired *BER* into the corresponding box, choose the chosen modulation and the tool will calculate the required *SNR* (see chapter 3.1.2.4).

The last thing that remains, is to pick the rest of the optical components. This should be done in an iterative manner, the cheapest components from the database should be chosen, with the worst performance, and if the calculations show, that the link will not be operational, components with better parameters should be picked. The link should be neither underdimensioned, nor overdimensioned, as the receiver could consequently be saturated or on the other hand the power margin could be too low, and the link would not have the required parameters (see chapter 2.4). The transmitter lens should be chosen based on the knowledge of the length of the link. The longer the link the smaller the divergence of the optical beam after the transmitter lens should be, to minimise the geometrical attenuation. The type of receiver should be chosen from the knowledge of the solar noise level and the received power. The lower the noise floor, the more sensitive detector can be used and the lower the received power level can be.

After the first iteration of the calculations, the optimal offset distance (see chapter 3.1.3) will be shown. To minimise the turbulent attenuation, the suggested offset should be added in the transfer chain definition window (see chapter 3.1.2.1).

When all of the attenuations have been minimised, the decision, whether an optical link in required conditions is feasible can be made.

3.2 Model situations

3.2.1 Example situation 1

The first model task is to design an underwater link between two submarines located near the equator, in the South Atlantic Ocean, at coordinates $0^{\circ}13'09.9''\text{S } 22^{\circ}57'45.2''\text{W}$. The link is to be operated on February 24, 2012, at 10:34. The submarines are both submerged 210 m under the surface of the sea. They are 170 m away from each other and we know from measurements, that 10 m from the first submarine a weak, 10 m long turbulence is located. The data should be transmitted at bitrate $R_b = 1\text{Gbit} \cdot \text{s}^{-1}$. The *BER* of the transmission should be kept under $1 \cdot 10^{-7}$.

- The communication will be realised in horizontal direction.
- The optimal, least attenuated wavelength selected by the tool is $\lambda = 565 \text{ nm}$.
- For given parameters and after selecting the transmitter with closest wavelength, for example modulation RZ-OOK can be used and the required $SNR = 17,34 \text{ dB}$.

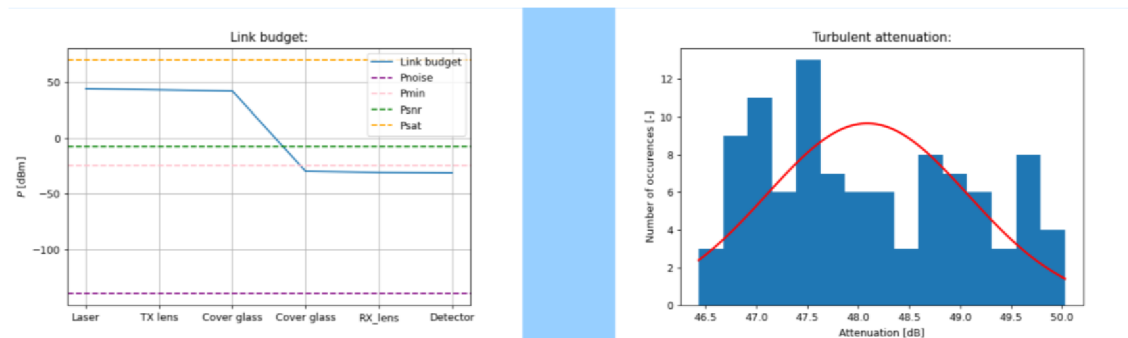
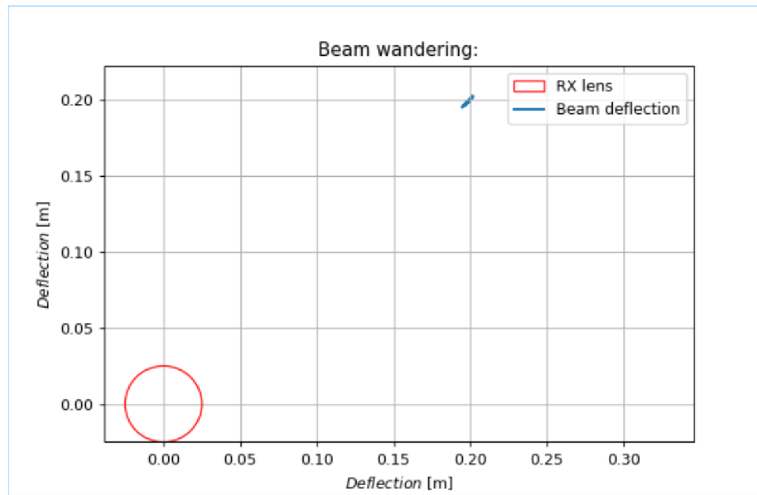


Figure 34: Calculated link budget after the first iteration (left side), calculated histogram for turbulent attenuations (right side).



Turbulent attenuation: 48.09 dB
 Propagation loss: 10.55 dB
 Attenuation by medium: 12.1 dB
 Total attenuation: 75.1 dB
 Background solar noise level: -139.21 dBm
 Received power: -31.12 dBm
 Link availability: 0.0 %
 Maximum bitrate: 0.0 Gbit·s⁻¹
 Link price: 303.12 US\$

To maximise link availability, moving the receiver by 198.0 mm in x-axis and by 198.0 mm in y-axis is recommended

Figure 35: Calculated beam wandering after the first iteration (top side), calculated parameters of the link (bottom side).

From the link budget in the Fig. 34 the user can see that the attenuation of the link is too high, and the received power is not within the required margin and from the histogram, the user can tell, that the turbulent attenuation in given conditions is relatively constant, around 48 dB. From the Fig. 35, it is apparent that the turbulent attenuation can be minimised by moving the receiver by 198 mm in x-axis and by 198 mm in y-axis. A filter does not need to be used, as the noise level is far below the received power.

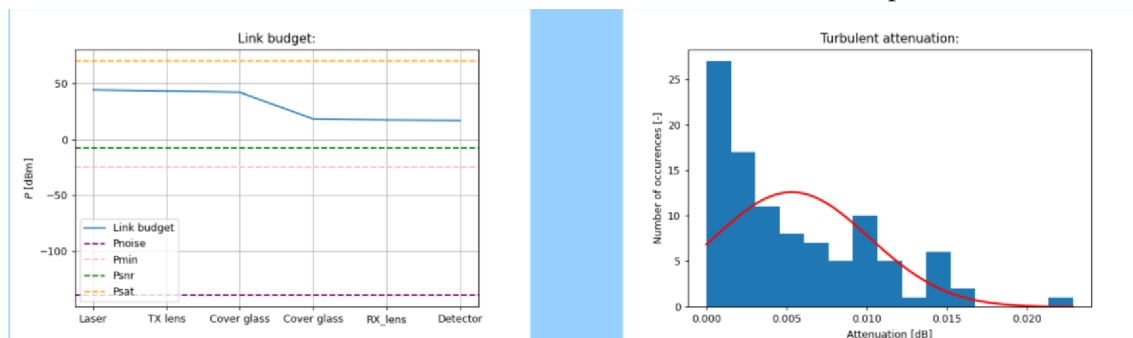


Figure 36: Calculated link budget after the second iteration (left side), calculated histogram for turbulent attenuations (right side).

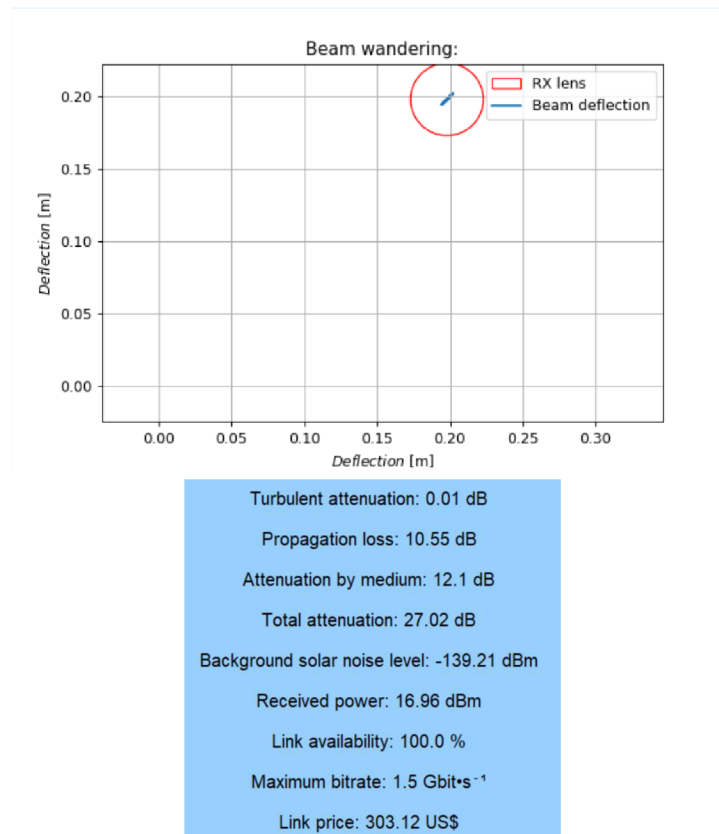


Figure 37: Calculated beam wandering after the second iteration (top side), calculated parameters of the link (bottom side).

From the link budget and from the histogram in the Fig. 36 the user can see that the attenuation of the link has dropped nearly to zero, because the turbulence is weak and thus the dynamics of the beam wandering (Fig. 37) is low allowing the receiving lens to receive almost all of the transmitted power. The power margin of the link is around 20 dB, which means that a lower power transmitter could be used, reducing the cost of the link. It is also apparent, that the requirements for the link were met.

3.2.2 Example situation 2

The second model task is to design an underwater link between a camera located at the ocean's bed and a buoy floating on the surface of the ocean above the sensor. The link shall be situated near the coast of Florida, in the Gulf of Mexico, at coordinates $27^{\circ}24'07.7''N$ $83^{\circ}30'48.1''W$. The link is to be operated on August 13, 2024, at 14:32. The sensor is located 92 m deep under the surface of the sea. The receiver is attached to the buoy, 50 cm under the surface of the sea. We know from measurements, that 13 m under the buoy a strong, 25 m long area of streams is located. The data should be transmitted at bitrate $R_b = 0,5 \text{ Gbit} \cdot \text{s}^{-1}$. The BER of the transmission should be kept under $3 \cdot 10^{-5}$.

- The communication will be realised in vertical direction, upwards.
- The optimal, least attenuated wavelength selected by the tool is $\lambda = 543 \text{ nm}$.
- For given parameters and after selecting the transmitter with closest wavelength, for example modulation 8-PPM can be used and the required $SNR = 7,29 \text{ dB}$.

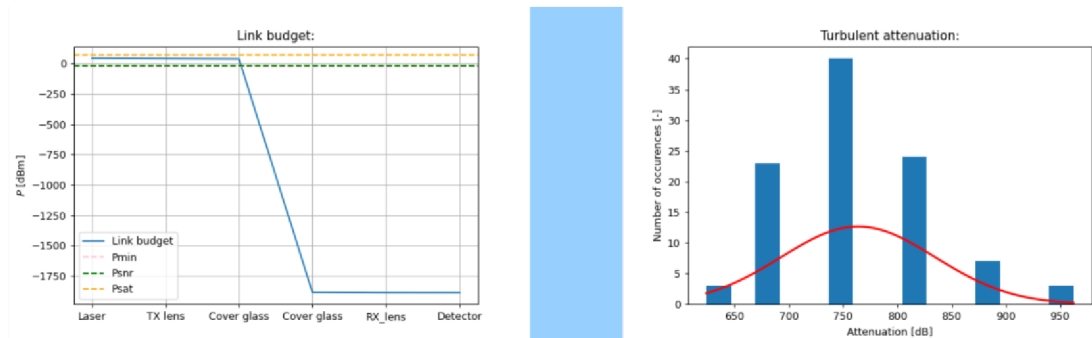


Figure 38: Calculated link budget after the first iteration (left side), calculated histogram for turbulent attenuations (right side).

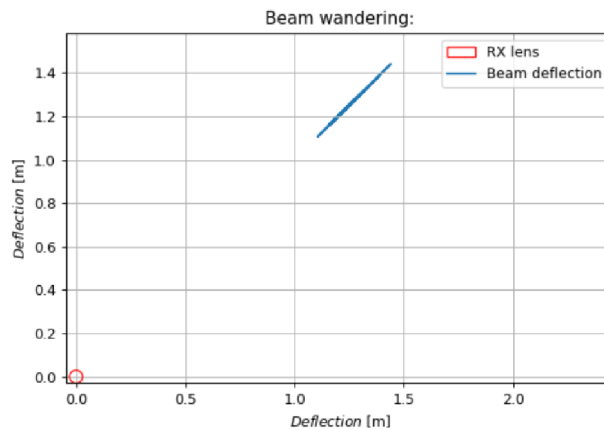


Figure 39: Calculated beam wandering after the first iteration .

From the link budget in the Fig. 38 the user can see that the attenuation of the link is too high, and the received power is not within the required margin and from the histogram, the user can tell, that the turbulent attenuation in given conditions changes a lot, it has variance over 300 dB. From the Fig. 39, it is apparent that the turbulent attenuation can

be minimised by moving the receiver by 1210 mm in x-axis and by 1210 mm in y-axis, which is caused by the fact, that the link is very long, and the underwater streams are strong. A filter does not need to be used, as the receiver is blocking all the light coming from the sun.

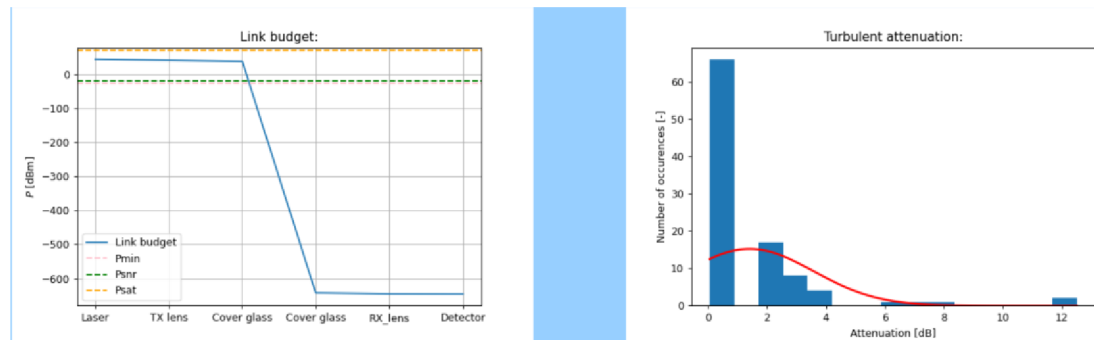


Figure 40: Calculated link budget after the second iteration (left side), calculated histogram for turbulent attenuations (right side).

Turbulent attenuation: 1.02 dB
Propagation loss: 14.15 dB
Attenuation by medium: 661.5 dB
Total attenuation: 689.03 dB
Received power: -645.05 dBm
Link availability: 0.0 %
Maximum bitrate: 0.0 Gbit·s ⁻¹
Link price: 304.12 US\$

Figure 41: Calculated parameters of the link.

From the link budget in the Fig. 40, it is apparent, that the designed link by far does not meet the requirements even after minimising the turbulent attenuation. This is caused, if the user looks at the Fig. 41, by the fact that the link is situated in S9 type of water, where the concentration of chlorophyll is very high and the link is also quite long, causing in consequence the attenuation by medium be extremely high. The desired link in these conditions cannot be realised.

3.2.3 Example situation 3

The third model task is to design an underwater link between a ship located at the surface of the ocean and an underwater station located at the ocean's bed. The link shall be situated in the Mediterranean Sea, at coordinates $34^{\circ}54'15.5''\text{N } 19^{\circ}15'39.7''\text{E}$. The link is to be operated on July 08, 2008, at 11:12. The station is located 86 m deep under the surface of the sea. The receiver is attached to the bottom of the ship, 8 m under the surface of the sea. We know from measurements, that 50 m under the ship a medium-strength, 3 m long area of streams is located. The data should be transmitted at bitrate $R_b = 1,2 \text{ Gbit} \cdot \text{s}^{-1}$. The BER of the transmission should be kept under $8 \cdot 10^{-4}$.

- The communication will be realised in vertical direction, downwards.
- The optimal, least attenuated wavelength selected by the tool is $\lambda = 500 \text{ nm}$.
- For given parameters and after selecting the transmitter with closest wavelength, for example modulation NRZ-OOK can be used and the required $SNR = 7,29 \text{ dB}$.

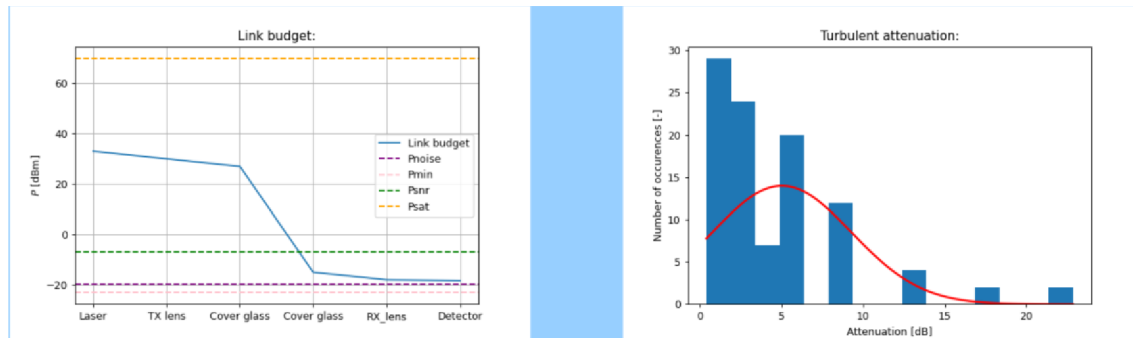


Figure 42: Calculated link budget after the first iteration (left side), calculated histogram for turbulent attenuations (right side).

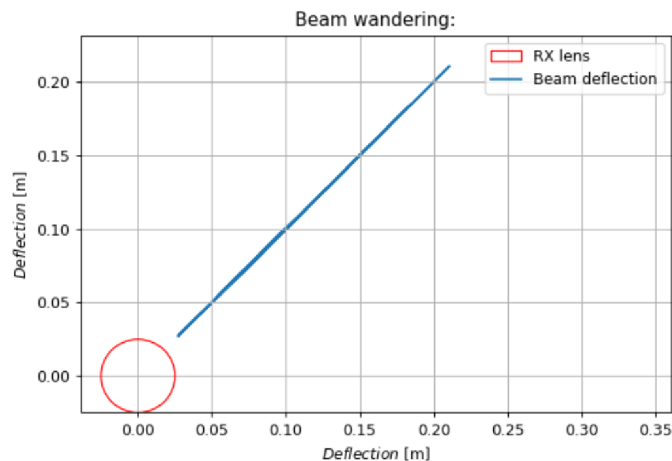


Figure 43: Calculated beam wandering after the first iteration.

From the link budget in the Fig. 42 the user can see that the solar noise level is too high, which means that the use of an optical filter before the receiver is mandatory. It can also be said that the attenuation of the link is too high, and the received power is not

within the required margin and from the histogram, the user can tell, that the turbulent attenuation in given conditions is relatively small and has variance around 15 dB. From the Fig. 43, it is apparent that the turbulent attenuation can be minimised by moving the receiver by 90 mm in x-axis and by 90 mm in y-axis. Further improvement can be reached by using a more sensitive receiver.

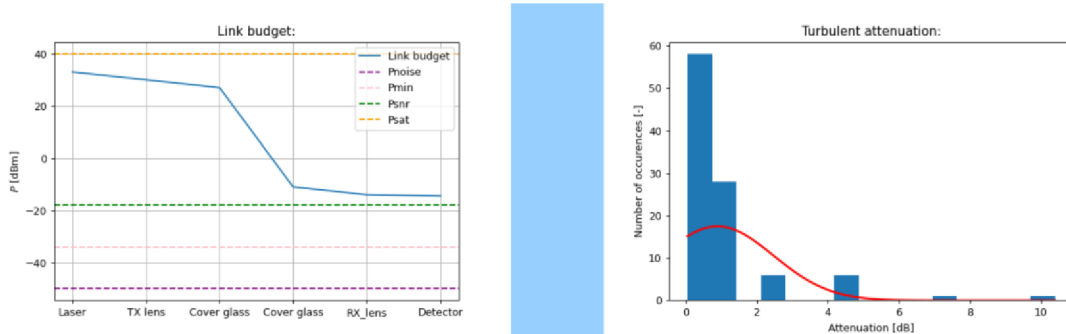


Figure 44: Calculated link budget after the second iteration (left side), calculated histogram for turbulent attenuations (right side).

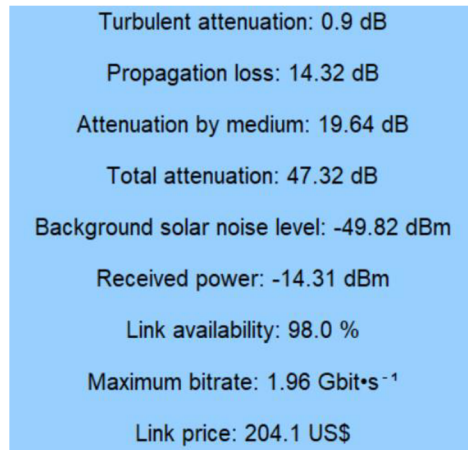


Figure 45: Calculated parameters of the link.

From the link budget in the Fig. 44, it is apparent, that the designed link meets after the second iteration the requirements. The turbulent attenuation has been minimised, solar noise level has been decreased, the sensitivity of the receiver has been increased and the required received power has been lowered. The desired link in these conditions can be realised with desired parameters, as can be seen from the Fig. 45.

4. CONCLUSION

The behaviour of the optical ray propagation under water has been investigated. A brief description of the characteristics of an underwater environment is presented, including description of absorption, scattering, turbulence, noises and chlorophyll concentration. Methods usable for the calculation of the deflection of the optical beam by turbulence are presented, including the application of Snell's law and ABCD ray tracing matrices. A thorough description of the procedure for calculating the extinction coefficient and solar noise is provided. Procedure for combining all the attenuating factors and calculating the received power by the receiver is shown. The algorithm for calculating link budget of an optical link, including all of the above mentioned procedures is implemented.

The turbulent space has a significant influence on the power received by the receiver. The factors that mainly decide how much the signal will be attenuated by the turbulent space are the length of the turbulent space, the angles in x and y axis at which the optical beam enters the turbulence, the length of the optical link and the size and position of the receiving lens. If the optical beam enters the turbulence along the optical axis of the system, it does not get deflected by the turbulence. The turbulent attenuation is strongly dependent on the chosen parameters of the optical cells, that can vary quickly in the turbulent space, depending on the strength of the turbulence and the resulting turbulent attenuation has a wide variance. To suppress the turbulent attenuation, bigger receiving lens can be used, or the receiver can be moved away from the optical axis into the mean distance, by which the optical ray is deflected by the turbulence in both axes.

It is apparent from the simulations, that the maximal attainable length of the link is mainly decided by the concentration of chlorophyll in the water. In areas where its concentration is high (especially coastal areas of higher water types), the maximum length of the link is in tens of meters, especially if the direction of the link is vertical and so the optical beam crosses the DCM (see chapter 1.4.6). If the concentration of chlorophyll is low or close to zero, away from the coastal areas and deep underneath the surface of the sea, the maximum length of the link is decided mainly by the geometrical attenuation, that is given by the divergence of the optical beam. The longer the link shall be the lower the divergence of the beam should be kept by using an appropriate transmitting lens to form the beam accordingly. The turbulent attenuation can be minimised by moving the receiver into the optimal position, if the dynamics of the turbulence is too high, this approach will not work, as the variance of the beam deflection would be too high for the receiving lens to receive enough power. To maximise the power received, receiving lens with bigger diameter can be used. If the received power is too low for the designed link to operate with desired parameters and the noise level is below the received power, a more sensitive receiver can be used, that requires lower number of photons to operate. If the noise level is high and this approach cannot be used, the noise level can be decreased by using an appropriate filter before the receiver or the link can be situated deeper into the ocean, if possible, where the solar irradiance is lower.

This is a theoretical work and the next step that should be taken would be to confront the results obtained from the calculations with measurements of real world applications.

LITERATURE

- [1] KOVALOVA, A.; HUDCOVA, L. a ROKA, R. Optical Ray Transfer Matrix Model of the Turbulent Cells Cascade. Online. *Radioengineering*. 2022, roč. 31, č. 4, s. 520-526. ISSN 1210-2512. Dostupné z: <https://doi.org/10.13164/re.2022.0520>. [cit. 2023-12-21].
- [2] HOVEM, Jens M., BEGHI, Marco G., ed. *Ray Trace Modeling of Underwater Sound Propagation*. 1. Rijeka, Croatia: nTech - Open Access Publisher, 2013. ISBN 978-953-51-1189-4. [cit. 2023-12-21].
- [3] H. Kaushal and G. Kaddoum, "Underwater Optical Wireless Communication," in *IEEE Access*, vol. 4, pp. 1518-1547, 2016, doi: 10.1109/ACCESS.2016.2552538. [cit. 2023-12-22].
- [4] AL-SHAMMA'A, A.I.; SHAW, A. a SAMAN, S. Propagation of Electromagnetic Waves at MHz Frequencies Through Seawater. Online. *IEEE Transactions on Antennas and Propagation*. 2004, roč. 52, č. 11, s. 2843-2849. ISSN 0018-926X. Dostupné z: <https://doi.org/10.1109/TAP.2004.834449>. [cit. 2023-10-02].
- [5] LANZAGORTA, Marco. *Underwater communications*. Synthesis lectures on Communications. 2013. ISBN 978-1-60845-844-8.
- [6] HUDCOVA, Lucie a WILFERT, Otakar. Calculation of the Applicable Wavelengths in Underwater Communication. Online. *2021 20th International Conference on Microwave Techniques (COMITE)*. 2021, s. 1-5. ISBN 978-1-6654-1454-8. Dostupné z: <https://doi.org/10.1109/COMITE52242.2021.9419881>. [cit. 2023-12-20].
- [7] GERRARD, A. a Burch, J. M. *Introduction to Matrix Methods in Optics-Dover Publication*. 1975. ISBN 0-486-68044-4.
- [8] KOVALOVA, Alzbeta a HUDCOVA, Lucie. Reciprocity of the Turbulent Cascade Model. Online. *2022 32nd International Conference Radioelektronika (RADIOELEKTRONIKA)*. 2022, s. 1-4. ISBN 978-1-7281-8686-3. Dostupné z: <https://doi.org/10.1109/RADIOELEKTRONIKA54537.2022.9764902>. [cit. 2023-12-22].
- [9] GUO, Yujian; TRICHILI, Abderrahmen; ALKHAZRAGI, Omar; ASHRY, Islam; NG, Tien Khee et al. On the Reciprocity of Underwater Turbulent Channels. Online. *IEEE Photonics Journal*. 2019, roč. 11, č. 2, s. 1-9. ISSN 1943-0655. Dostupné z: <https://doi.org/10.1109/JPHOT.2019.2898094>. [cit. 2023-12-22].
- [10] CHANCEY, M.A. *Short Range Underwater Optical Communication Links*. M.S.Thesis. Raleigh, NC, USA: Dept. Elect. Eng., North Carolina State Univ., 2005.
- [11] Vladimir I. Haltrin, "Chlorophyll-based model of seawater optical properties," *Appl. Opt.* **38**, 6826-6832 (1999)
- [12] JOHNSON, Laura J.; GREEN, Roger J. a LEESON, Mark S. Underwater optical wireless communications: depth dependent variations in attenuation. Online. *Applied Optics*. 2013, roč. 52, č. 33, s. 1-5. ISSN 1559-128X. Dostupné z: <https://doi.org/10.1364/AO.52.007867>. [cit. 2023-12-23].

- [13] BRICAUD, Annick; BABIN, Marcel; MOREL, André a CLAUSTRE, Hervé. Variability in the chlorophyll-specific absorption coefficients of natural phytoplankton: Analysis and parameterization. Online. *Journal of Geophysical Research: Oceans*. 1995, roč. 100, č. C7, s. 13321-13332. ISSN 0148-0227. Dostupné z: <https://doi.org/10.1029/95JC00463>. [cit. 2023-12-23].
- [14] L. J. Johnson, "The underwater optical channel", 2012, [online] Available: http://www2.warwick.ac.uk/fac/sci/eng/study/pg/students/esrlab/publications/factors_affecting_light_underwater.pdf.
- [15] ANDREWS, Larry C. a PHILLIPS, Ronald L. Laser Beam Propagation through Random Media. Online. Roč. 2005, s. 1-22. Dostupné z: <https://doi.org/10.1117/3.626196>. [cit. 2023-12-23].
- [16] HUDCOVA, Lucie a WILFERT, Otakar. Quantification of the atmospheric turbulence by the method of the equivalent temperature gradient. Online. *2018 28th International Conference Radioelektronika (RADIOELEKTRONIKA)*. 2018, roč. 28, s. 1-4. ISBN 978-1-5386-2485-2. Dostupné z: <https://doi.org/10.1109/RADIOELEK.2018.8376401>. [cit. 2023-12-27].
- [17] *Optical Receiver Noise*. Online. Optical Receiver Noise. 2020. Dostupné z: <https://www.fiberoptics4sale.com/blogs/wave-optics/optical-receiver-noise>. [cit. 2023-12-27].
- [18] BLAUNSTEIN, Nathan; ENGELBERG, Shlomo; KROUK, E. a SERGEEV, Mikhail. Fiber Optic and Atmospheric Optical Communication. Online. Dostupné z: <https://doi.org/10.1002/9781119602019>. [cit. 2023-12-27].
- [19] SIMPSON, Jim A.; HUGHES, Brian L. a MUTH, John F. A spatial diversity system to measure optical fading in an underwater communications channel. Online. *OCEANS 2009*. 2009, s. 1-6. ISBN 978-1-4244-4960-6. Dostupné z: <https://doi.org/10.23919/OCEANS.2009.5422262>. [cit. 2023-12-27].
- [20] WEN, Yang Jing; CUI, Yan a BAI, Yusheng. Mitigation of optical multipath interference impact for directly detected PAMn system. Online. *Optics Express*. 2020, roč. 28, č. 25. ISSN 1094-4087. Dostupné z: <https://doi.org/10.1364/OE.413054>. [cit. 2023-12-27].
- [21] HUDCOVA, Lucie a KOVALOVA, Alzbeta. Calculation of Solar Noise in Selected Underwater Depths. Online. *2022 32nd International Conference Radioelektronika (RADIOELEKTRONIKA)*. 2022, s. 01-06. ISBN 978-1-7281-8686-3. Dostupné z: <https://doi.org/10.1109/RADIOELEKTRONIKA54537.2022.9764929>. [cit. 2023-12-28].
- [22] HAMZA, Tasnim; KHALIGHI, Mohammad-Ali; BOURENNANE, Salah; LÉON, Pierre a OPDERBECKE, Jan. Investigation of solar noise impact on the performance of underwater wireless optical communication links. Online. *Optics Express*. 2016, roč. 24, č. 22. ISSN 1094-4087. Dostupné z: <https://doi.org/10.1364/OE.24.025832>. [cit. 2023-12-28].
- [23] SOGANDARES, Frank M. a FRY, Edward S. Absorption spectrum (340–640 nm) of pure water I Photothermal measurements. Online. *Applied Optics*. 1997,

- roč. 36, č. 33. ISSN 0003-6935. Dostupné z:
<https://doi.org/10.1364/AO.36.008699>. [cit. 2024-01-01].
- [24] BASHKATOV, Alexey N.; GENINA, Elina A. a TUCHIN, Valery V.
<title>Water refractive index in dependence on temperature and wavelength: a simple approximation</title>. Online. S. 393-395. Dostupné z:
<https://doi.org/10.1117/12.518857>. [cit. 2024-01-02].
- [25] WAXLER, R.M. a WEIR, C.E. Effect of pressure and temperature on the refractive indices of benzene, carbon tetrachloride, and water. Online. *Journal of Research of the National Bureau of Standards Section A: Physics and Chemistry*. 1963, roč. 67A, č. 2. ISSN 0022-4332. Dostupné z:
<https://doi.org/10.6028/jres.067A.016>. [cit. 2024-01-02].
- [26] *Edmund Optics*. Online. Edmund Optics. 2024. Dostupné z:
<https://www.edmundoptics.com/f/785nm-laser-line-coated-plano-convex-pcx-lenses/14214/>. [cit. 2024-05-20].
- [27] *Thorlabs*. Online. Thorlabs. 2024. Dostupné z:
https://www.thorlabs.com/newgrouppage9.cfm?objectgroup_id=859&pn=SA200-2B. [cit. 2024-05-20].
- [28] FUQIN Xiong, *Digital Modulation Techniques, Second Edition*, Artech, 2006. Dostupné z: <https://ieeexplore.ieee.org/abstract/document/9101102>. [cit. 2024-05-20].

LIST OF SYMBOLS AND ABBREVIATIONS

Abbreviations:

FEKT	Fakulta elektrotechniky a komunikačních technologií
VUT	Vysoké učení technické v Brně
DCM	Deep chlorophyll maximum
SNR	Signal to noise ratio
BER	Bit error rate

Symbols:

λ	wavelength	(nm)
$\Delta\lambda$	bandwidth of the filter	(nm)
n	refractive index	(-)
v	velocity	(m · s ⁻¹)
a	attenuation coefficient	(m ⁻¹)
b	scattering coefficient	(m ⁻¹)
L	attenuation	(-)
G	gain	(-)
ω	angular frequency	(rad · s ⁻¹)
ϵ	permittivity	(F · m ⁻¹)
f	frequency	(Hz)
C_c	concentration of chlorophyll	(mg · m ⁻³)
C_F	concentration of fulvic acid	(mg · m ⁻³)
C_H	concentration of humic acid	(mg · m ⁻³)
σ	standard deviation	(-)
P	power	(W)
H_0	DC gain of the communication channel	(-)
A_{PD}	surface area of the photodetector	(m ²)
R	curvature radius	(m)
t	thickness	(m)
l	length	(m)
I	optical intensity	(W · m ⁻²)
w_0	waist radius	(m)
z_0	Rayleigh length	(m)
d	side length of the receiving lens	(m)
R_b	bitrate of the communication	(bit · s ⁻¹)

LIST OF APPENDICES

APPENDIX A - FLOWCHART OF THE MAIN ALGORITHM	60
APPENDIX B - THE SOURCE CODE	61

Appendix A - Flowchart of the main algorithm

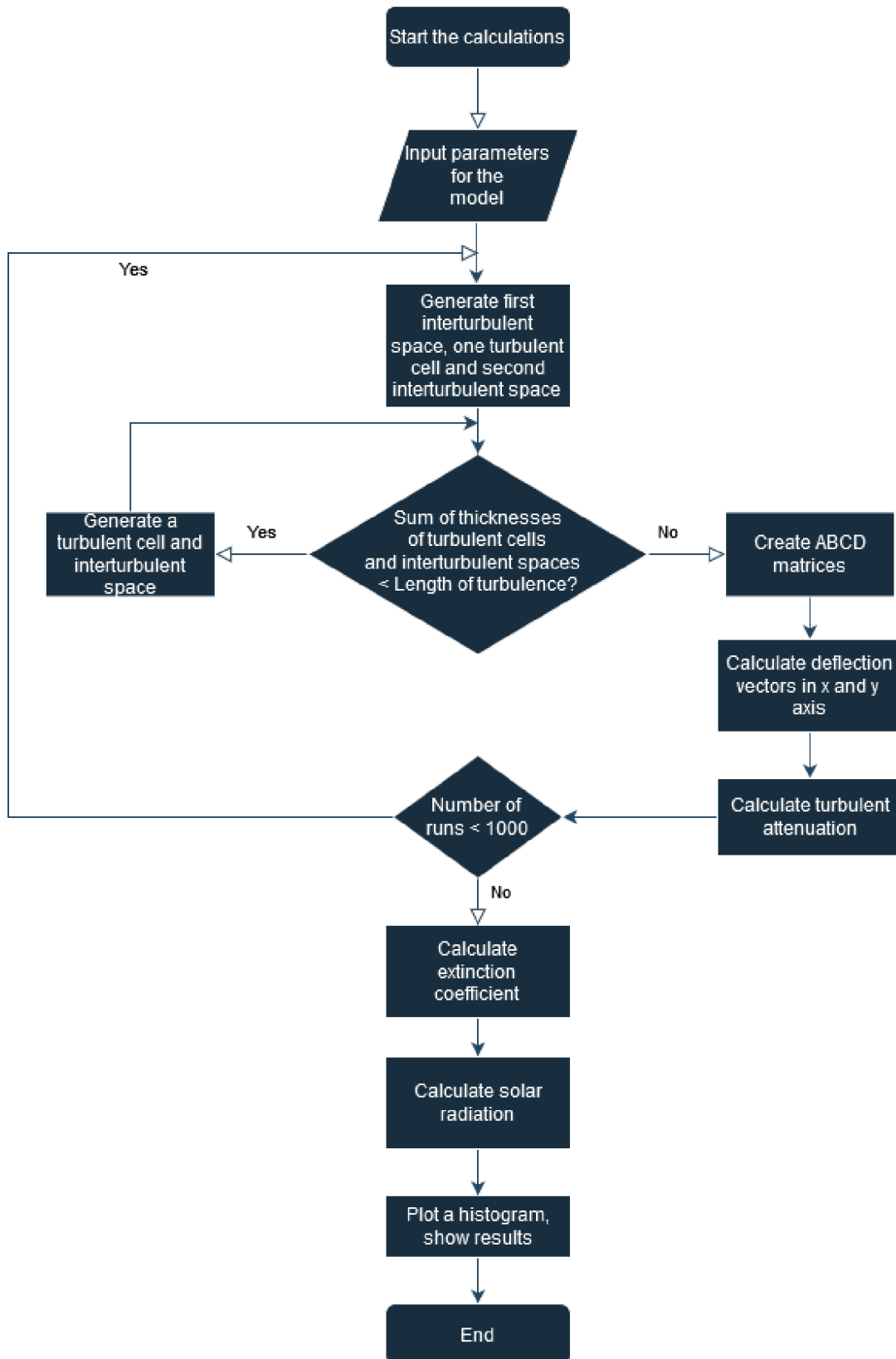


Figure 46: Flowchart of the algorithm for calculating turbulent optical ray attenuation.

Appendix B - The source code

The source code can be found at the attachments to the text of the thesis. For the program to correctly work, python libraries “numpy”, “scipy”, “Tkinter”, “Pandas”, “Pillow”, “netCDF4”, “solarpy”, “datetime”, “timezonefinder”, “pytz”, “os”, “sys” and “matplotlib” need to be installed. This program was tested and optimized with Python version 3.12.1, on computer running on Windows 10 and 11 with 8 GB of RAM. The dependencies can be installed automatically by the included batch file “setup.bat”. If for some reason the file gets detected by an antivirus software, Python needs to be installed manually and after opening the file “setup.bat”, the last lines marked as “Install libraries using pip” need to be executed from command line.